UNIVERSITY OF CAPE TOWN

Heat and Mass Transfer Effects of Ice Growth Mechanisms in Water and Aqueous Solutions

Michael Kapembwa

February, 2013

Heat and Mass Transfer Effects in Ice Growth Mechanisms in Water and Aqueous Solutions

Michael Kapembwa

Kpmmic003

Submitted in fulfilment of the requirements for the Degree of

Master of Science in Engineering

Department of Chemical Engineering

University of Cape Town

Cape Town, South Africa.

Supervisors:

Dr Dyllon G. Randall

Dr Marcos Rodriguez-Pascual

Prof. Alison E. Lewis

February, 2013

“Unless the LORD had been my help, my soul had almost dwelt in silence”

This work is dedicated to my late brother Forbes Kapembwa for his invaluable sacrifice for me and my family

---

“I know the meaning of plagiarism and declare that all work in this document, save for that which is properly acknowledged, is my own”

Acknowledgements

I would like to express my sincere gratitude to my supervisors Prof. A.E Lewis, Dr M. Rodriguez-Pascual and Dr D.G. Randall for their supervision and involvement in my project. I appreciate the time and effort spent on my project and their investment into my research skills. To Miss Christine Olsen and Dr Tracy-Ann Craig, thanks for providing materials and equipment needed for my research work.

I would like to also thank the Physics Department for accommodating me in the Optics lab where parts of my experiments were conducted. Thanks to Leslie and Jeff.

To the greatest research team of all times (CPU), you guys simply rock! The late nights, academic, cultural and political talks have given me more insight in many things and have allowed me to appreciate the diversity of the world we live in. Thanks for your friendship and contribution to my work.

To my friends Bernard and Fridah, Nicholas and Luse, Mwenya, Gladwell and Robin Benjamin, thanks for making my stay in Cape Town memorable. Your company, encouragements and prayers will forever be appreciated. To Noah and Emeldah, thanks for your friendship. To all of you, your words of wisdom on many things especially my personal life are greatly appreciated.

To my fiancée, Thelma and my sisters, Petronella and Salome, my brothers'-in-law William and Raymond, to Mum (Mrs Rose Kasweshi), thanks for your love and support. At no time have I ever doubted your belief in me .To Mbulawa, your late-night calls were always refreshing and to my late brothers and sister, your love and support will always be remembered.

Finally, I am forever grateful to my heavenly Father, who means everything to me.

Abstract

Research into ice crystallization processes is an important area of study. The desire to improve product quality and efficiency of processes involving ice crystallization in industries such as desalination by freezing, freeze drying, freeze concentration and freeze crystallization for food processing, requires insight into the ice growth mechanisms. More so, a novel technology called Eutectic Freeze Crystallization, where water is recovered in the form of ice, requires that ice crystals are of high purity as this directly determines the quality of the water obtained. During ice crystallization, ice growth mechanisms play an important role in determining the structure, size and morphology of ice which have an effect on separation processes and product purity. Heat and mass transfer play a fundamental role in ice growth processes as they affect the thermodynamics and kinetics of the crystallization process.

Ice growth experiments were carried out in pure water, in 8.4 wt% and 16.8 wt% magnesium sulphate and in 8.4 wt% sodium nitrate using a 10x5x31 mm test cell made of Plexi-glass®. The Colour Schlieren optical technique was used to conduct the experiments. This is because of its capability to map refractive index gradients related to either temperature or/and concentration gradients of the solution during crystal growth.

It was observed that, contrary to current understanding, some of the heat of crystallization was transferred to the liquid side and the other part to the solid side. During dendritic growth, about 3%–16% of the heat of crystallization diffused into the liquid side of the growing interface and was responsible for the liquid temperature to increase during dendritic growth. This heat of crystallization was responsible for the melting of the dendrites before the initiation of layered growth. At the transition stage between dendritic growth and layer growth, a higher supersaturation was observed.

For a pure water system, it was found that the ice growth rate increased with a decrease in temperature on the liquid side near the interface. The high growth rate led to dendritic growth and occurred at early stages of crystal formation due to high

supersaturation. Once the metastable zone was broken, the supersaturation decreased and the lower growth rate resulted in layered growth.

When comparing ice surface temperature using two crystal growth models, differences were observed of 0.58 °C lower when compared to the values predicted by the Huige model and of 0.84 °C higher than the Kallungal model.

It was also observed that the ice growth rate in pure water was higher than in salt solution. This can be explained by the diffusion of solute concentration that retards the growth rate of ice in the solution due to the changes in thermodynamic properties of the front liquid.

This thesis has shown that heat transferred through the solution affects the temperature profiles, which affect the local supersaturation. The local supersaturation is also affected by the transfer of heat of crystallization during growth. The local supersaturation affects the ice growth rate and morphology. During ice growth in solution, the solute concentration retards the growth rate. Therefore, heat and mass transfer in solution during ice growth plays an important role in determining the ice growth processes.

Table of Contents

List of Figures

List of Tables

1 Introduction

1.1 Motivation

Water is essential for life and plays a vital role in the proper functioning of the Earth's ecosystems. Poor water quality, on the other hand, has many economic costs associated with it including degradation of ecosystem services; health-related costs; impacts on economic activities such as agriculture, industrial production, tourism, and increased water treatment cost (Palaniappan et al., 2010).

Fresh, good-quality water is under stress due to various industrial and human activities. Urbanisation, population growth, and climate change are some of the factors threatening the quality and quantity of water. Industrial activities such as mining have the potential to cause widespread environmental damage on numerous fronts (Hilson, 2000; Palaniappan et al., 2010). The water can be affected through its heavy use in ore processing, pollution from discharged mine effluent and seepage from tailings and waste rock impoundments.

Effective and sustainable solutions to water quality challenges are thus needed by the development and improvement of novel technologies that can treat stream discharges. This would reduce the load on the freshwater and the environment.

In view of the above challenge, a novel technology called Eutectic Freeze Crystallization (EFC) has the potential to treat metallurgical brines and inorganic industrial waste streams containing dissolved salts. Brine is a solution with high concentrations of dissolved salts. In the EFC process, both pure water in the form of ice and pure salts are simultaneously recovered from an inorganic waste stream as illustrated in Figure 1. This is achieved when the crystallization process is operated under eutectic conditions where both the ice and salt form simultaneously and the two phases separate due to their density differences.

The feasibility of conventional separation techniques such as evaporative crystallization, cooling crystallization, and reverse osmosis are often determined from considerations of the energy consumption, the attainable yield, and the nature and purity of the products (Van der Ham et al., 1998).

By using EFC, pure water and solid salt can be recovered at low energy costs and very high yields. The total salt and water recovery can be as high as 90% (Lewis et al., 2010). This changes the focus from cost to value by introducing a new separation process which uses a waste stream as unprocessed materials (Genceli, 2008).

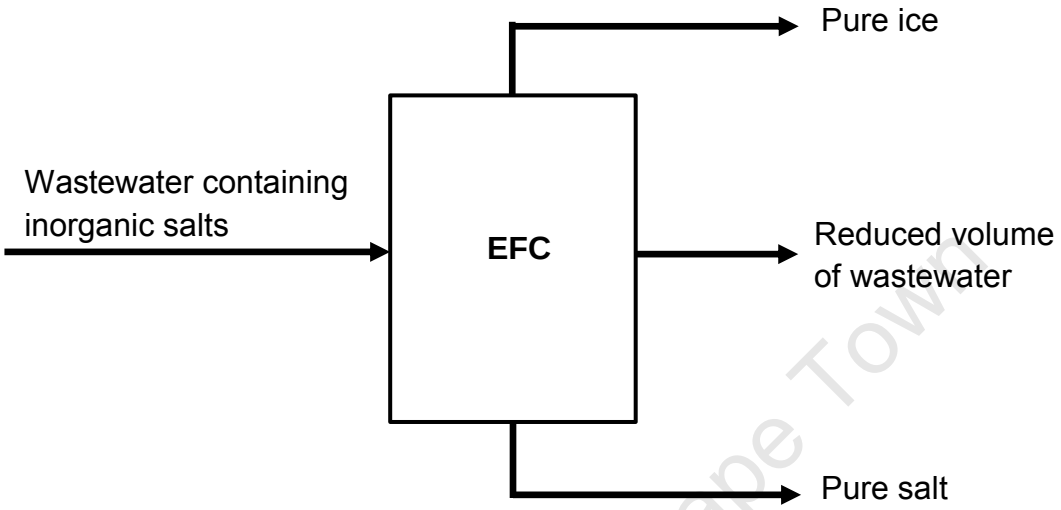

Figure 1: Schematic diagram of Eutectic Freeze Crystallization process

In order to obtain pure water, the ice crystals formed must be pure. However, as in other crystallization processes, there are various factors that affect the purity and quality of crystal products. Fundamentally, growth processes of ice crystals determine the quality of the ice formed. Therefore, this thesis aims to understand the coupled heat and mass transfer effects on ice growth processes as they are the principal processes occurring during crystal growth.

1.2 Project background

1.2.1 Description of Eutectic Freeze Crystallization

Eutectic Freeze Crystallization (EFC) is an extension of the freeze crystallization process and in principle, both organic and inorganic aqueous solutions can be separated (van der Ham et al., 1999).

1.2.2 Operating principle of ice crystallization in E.F.C process

The principle of EFC can be described using a phase diagram of a binary salt–water mixture, shown in Figure 2 (Rodriguez-Pascual, 2008).

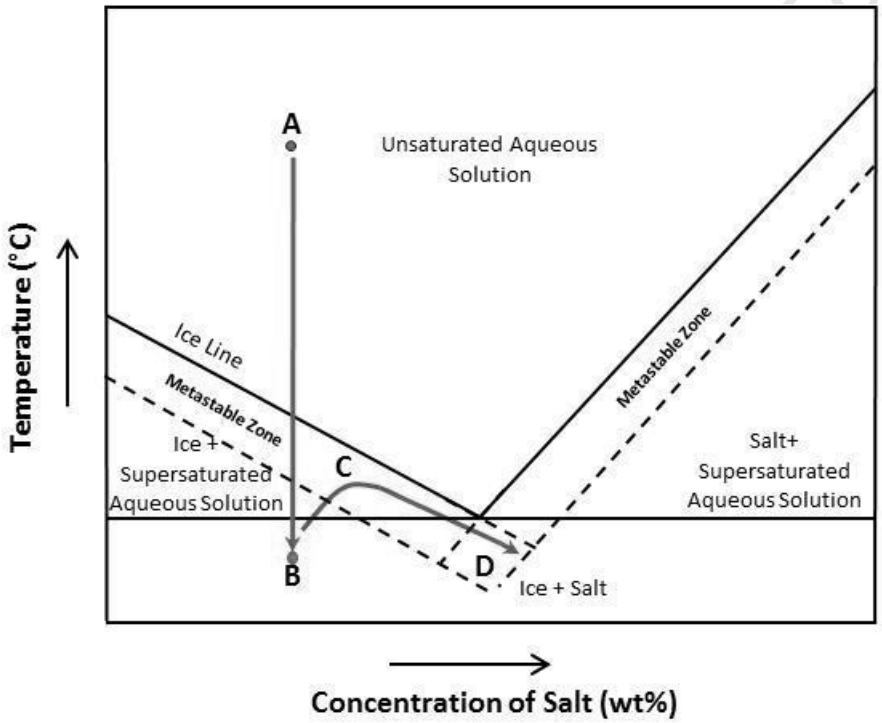

Figure 2: Binary phase diagram of a salt-water solution-adapted from (Adapted from Rodriguez-Pascual, 2008, p.5)

If a solution is in an unsaturated area with a concentration lower than eutectic composition **A** and is cooled down it would reach the solubility line (ice line). Continuous cooling will make the system cross the solubility line and become supersaturated within the metastable zone. In this region, no spontaneous nucleation will occur. If not seeded, ice only forms after the system has exceeded the

metastable zone width limit at point **B**. The temperature then increases up to point **C** due to the generation of the heat of crystallization. Further cooling decreases the temperature, and increases the concentration of the system as it approaches the metastable area of salt and eutectic conditions at **D**. Operating at point **D**, both the ice and the salt crystals will form simultaneously. Similarly, starting with a solution of higher concentration than the eutectic composition will result in the formation of salt first and then the ice when eutectic conditions are reached.

1.2.3 Advantages and disadvantages of EFC

- Compared to evaporative processes for brine treatment, freeze crystallization is less energy-intensive and environmentally friendly since both water and salt species are recovered from an inorganic stream. This is elaborated in the chart in Figure 3. Energy costs can be reduced by about 70% for certain systems (Van der Ham et al., 1998).
- The process does not require addition of chemical compounds (Lorain et al., 2001).
- The waste stream can be used as a resource (Genceli, 2008).

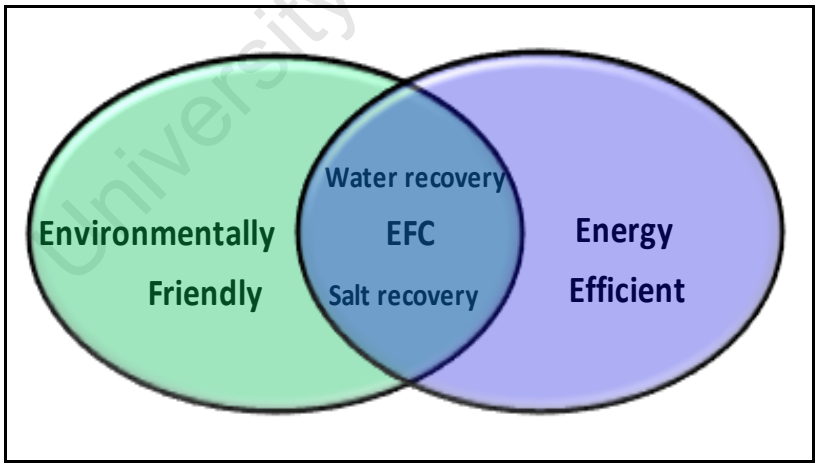

Figure 3: Advantages of Eutectic Freeze Crystallization

- The most significant disadvantages of EFC are the capital costs (two or three times those of distillation or evaporation systems and scale limitations, but these can be overcome as the technology develops (Randall, 2010).

- Another drawback of EFC is that the process suffers from fouling on the heat exchanger walls which affects heat transfer capacities and thus production capacities (Pronk et al., 2008).

1.2.4 Other areas where this study may be of interest

Other industrial areas this study may be of interest include:

- Food processing such as freeze drying and freeze concentration (Petzold & Aquilera, 2009).
- Desalination of water, thermal energy storage and solidification of castings in metallurgy and purification of materials (Grange et al., 1976).

1.3 Thesis overview

Below is the overview of the thesis according to the chapters.

i. Chapter 2: Theory and literature review

Chapter 2 underlines the basic and fundamental principles of crystallization narrowing to melt crystallization and more specifically, ice crystallization. The liquid phase as well as the solid–liquid interface are discussed in relation to temperature and concentration gradients due to heat and mass transfer effects, supersaturation, growth rate, morphology and ice purity. A detailed review on these parameters is discussed in line with the motivation and background. The chapter also includes the basic equations of irreversible thermodynamics and a review of the classical approach on heat and mass transport in non-equilibrium environments.

A Colour Schlieren technique, which is the basis of the methodology employed in this thesis, is discussed under the theory section describing what it is, how it operates and why it was chosen for this study.

ii. Chapter 3: Methodology

This chapter focuses on the details of the technique employed, set-up of the apparatus, how measurements were done and the process of quantitative analysis of the data. It also covers the materials used and the experimental procedure.

iii. Chapter 4: Results and discussion

The results for different investigations are presented with a brief description of what they are, how they were obtained followed by a detailed discussion. Two major sections are covered, i.e. the analysis of ice grown in pure water and in a salt solution.

iv. Chapter 5: Conclusions and recommendations

Conclusions are drawn based on the set objectives and the hypothesis. Recommendations based on experiences during the research studies are proposed and a highlight of future works worth undertaking.

2 Theory and literature review

2.1 Theory

2.1.1 Crystallization in general

The term crystallization, as known in the chemical industry, refers to the formation of a dispersed solid phase from a fluid that is either a solution or an impure melt (Mullin, 2001). It is one of the oldest unit operations in the portfolio of industrial and/or laboratory separation whose other possible functions include purification, concentration and solidification (Ulrich & Stelzer, 2011). Few branches of chemical and process industries do not, at some stage, use crystallization for production or separation purposes. For example, crystallization is used in the manufacture of crystalline products of pharmaceutical, organic fine chemical and dye industries. It is also a key operation in the desalination of seawater, concentration of fruit juices and the removal of unwanted materials or recovery of valuable constituents in many industrial processes (Mullin, 2002). Figure 4 shows some of the general aspects involved in crystallization (Ulrich & Stelzer, 2011).

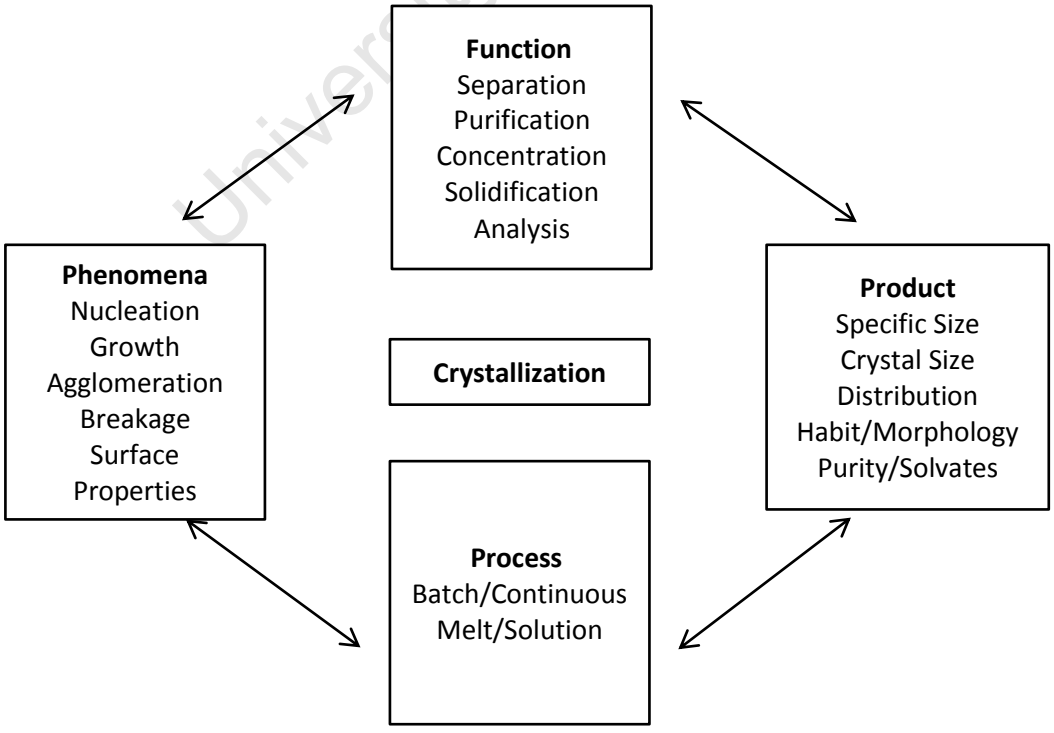

Figure 4: Different aspects involved in crystallization (Ulrich & Stelzer, 2011, p.2)

Crystallization is governed by very complex, interacting variables. It is a simultaneous heat and mass transfer process with a strong dependence on fluid and particle mechanics (Mullin, 2002).

2.1.2 Supersaturation

The thermodynamic driving force for crystallization is called supersaturation. It is defined as a deviation from thermodynamic equilibrium (Ulrich & Stelzer, 2011). The degree of supersaturation can be expressed in terms of chemical potential, concentration or temperature.Table 2-1 presents a summary of different expressions of supersaturation.

Table 2-1: Expressions of supersaturation

Expression	Description	Formula
Chemical potential $\Delta\mu$	Difference between the chemical potential of the system μ and the chemical potential of saturation μ*, where μ(C,T)	μ-μ*
Concentration ΔC	Difference between the solute concentration C and the concentration at equilibrium C^*	$C-C^*$
Temperature ΔT	Difference between the system temperature at equilibrium T^* and the actual temperature T	T^*-T

Other common expressions are the supersaturation ratio S and the relative supersaturation σ which are both dimensionless:

$$S = C/C^* \qquad \text{Equation 2-1}$$

$$\sigma = \Delta C/C^* = S - 1 \qquad \text{Equation 2-2}$$

The local supersaturation depends on solution temperature and the presence of the growing crystals due to the release of heat of crystallization (Mersmann, 2001).

In order to maintain good yields and high product purity, it is desirable to maintain a constant supersaturation throughout the crystallization process especially in the case of batch processes. This requires permanent adjustment of the driving force (Jones & Ulrich, 2006).

2.1.3 Metastable Zone

The metastable zone is a supersaturated region on the phase diagram where spontaneous nucleation is improbable. However, with addition of a seed crystal in this region, growth will occur (Jones & Ulrich, 2006; Dhanaraj et al., 2010). In contrast to the thermodynamically defined solubility curve, the metastable limit curve is not thermodynamically defined and is strongly dependent on process parameters such as the temperature level, rate of change of supersaturation, impurities present, or fluid dynamic (Ulrich & Stelzer, 2011). The metastable zone (MSZ) is an important concept in crystallization since it defines the operating region of a process. It is associated with better efficiency of crystallization processes such as separation and purification. This is because it enables the control of the shape and the size of crystalline products (Sangwal, 2011). In order to optimize the recovered ice purity, the operations are limited to within the metastable zone (Jones & Ulrich, 2006). Figure 5 shows a diagram illustrating the concept of the metastable zone (Mullin, 2002).

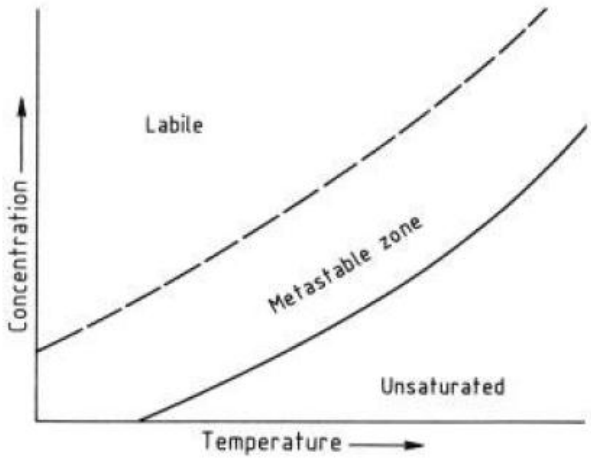

Figure 5: Solubility diagram showing Metastable Zone (Mullin, 2002, p.4)

2.1.4 Nucleation

Nucleation is the creation of crystalline bodies within a supersaturated fluid (Mullin, 2002). Nucleation and growth kinetics determine crystal characteristics like purity and morphology (Ulrich & Stelzer, 2011). There are two types of nucleation, primary nucleation and secondary nucleation. Primary nucleation occurs in the absence of seed crystals, whereas secondary nucleation occurs in the presence of seed crystals. Primary nucleation is difficult to control and unreliable, as it will not always occur at precisely the same supersaturation. This is not desirable as it leads to uncontrolled nucleation which yields poor crystal products. Hence, in order to produce high quality crystals in a reproducibly manner, secondary nucleation by means of seeding is the preferred method of inducing the crystallization process. The summary of the types of nucleation are presented in the Figure 6 below (Mullin, 2002).

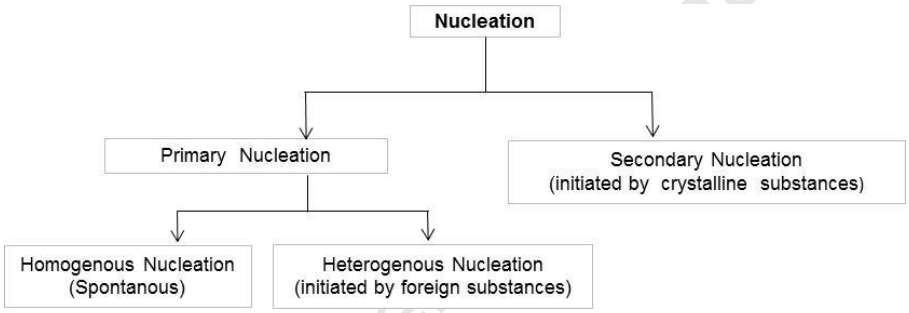

Figure 6: Types of nucleation (Mullin, 2002, pp. 12–14).

2.1.5 Crystal growth

Crystal growth is the enlargement of crystals caused by the deposition of matter on an existing surface in a supersaturated solution. It involves the mass transfer of molecules to the crystal surface as well as the removal of the heat of crystallisation which is released (Ayel et al., 2006). Once a stable nucleus has been created in a solution, it is capable of growing into a crystal. Crystal growth rates depend upon supersaturation and the nature of the fluid flow in the vicinity of the crystal surface (Jones & Ulrich, 2006). Fast crystal growth will result in a high yield over a specific time period. However, it is the most common cause of inclusion formation during crystallization processes (Mullin, 2002). Inclusions in crystallization are microscopic pockets in crystals that may contain impurities or air (Myerson, 2002).

2.2 Melt Crystallization

Ice crystallization in Eutectic Freeze Crystallization can be considered a type of melt crystallization. Melt crystallization is a separation and purification technique for chemical compounds and mixtures of metals. The difference between melt and solution crystallization is not precisely defined. However, in melt crystallization, the heat control is generally viewed as the rate determining step (Jones & Ulrich, 2006). The composition of the melt adjacent to the surface of the growing crystals is often controlled by the removal of heat of crystallization (Mersmann, 2001). However, in crystallization from a solution, the liquid solid phase change is dominated by mass transfer effects (Myerson, 2002).

Melt crystallization can be either a suspension or layer-based. In layered crystallization processes, crystals grow on a cooled surface and the crystalline product is separated from its residue melt by mechanical means (Mersmann, 2001). Figure 7 shows a crystalline layer growing on a cooled plate (Myerson, 2002). In suspension based melt crystallization, crystals formed are kept in suspension and are allowed to grow by sub-cooled temperature of the mother liquor.

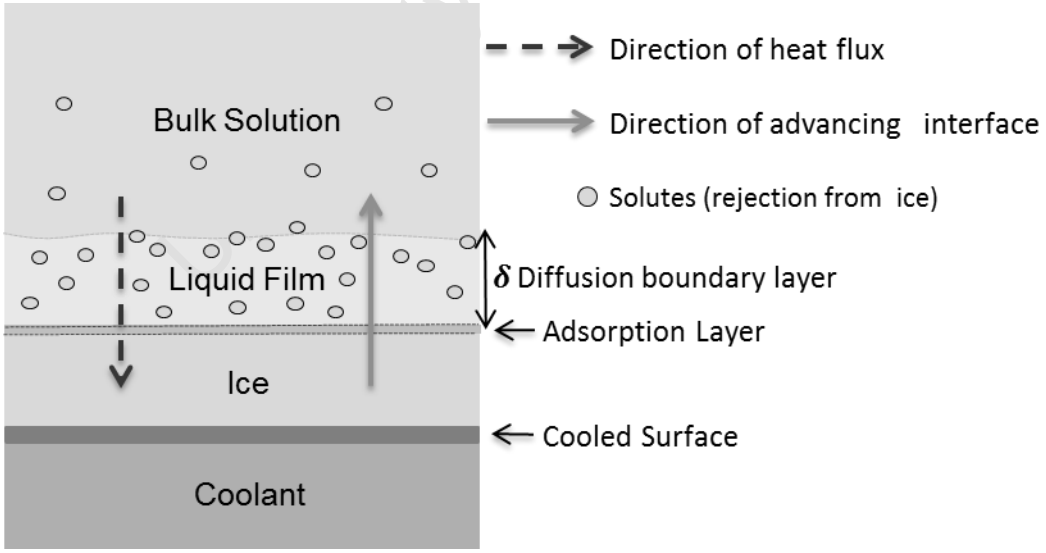

Figure 7: Ice Crystal: Solid–liquid interface (Adapted from Myerson, 2002, p.75)

In Figure 7, as crystallization takes place heat is released to the liquid and solid phase and the solutes diffuse from the ice phase through the diffusion boundary layer into the bulk solution. This occurs at the solid–liquid interface and the structure

of the interface may be smooth or rough depending on the level of supersaturation (Myerson, 2002) and the rate of heat removal. It has been postulated that partial rejection of impurities at the crystal-solution interface causes the concentration of impurities in the interfacial region to increase above its value in bulk solution. Thus, with increasing growth rates, impurities can be rejected at a rate faster than they can diffuse into the bulk solution resulting in their accumulation in the interfacial region (Myerson, 2002).

2.2.1 Temperature and concentration gradient at the solid–liquid interface

The process of solute rejection from the growing crystal into the bulk solution and the generation of heat of crystallization create temperature and concentration gradients at the solid–liquid interface as shown in Figure 8 (Myerson, 2000). These gradients affect the growth rate of the crystals and the amount of impurity inclusions. Temperature and concentration profiles are important parameters for determining impurity behaviour in the growth of the crystalline layer (Kim & Ulrich, 2001).

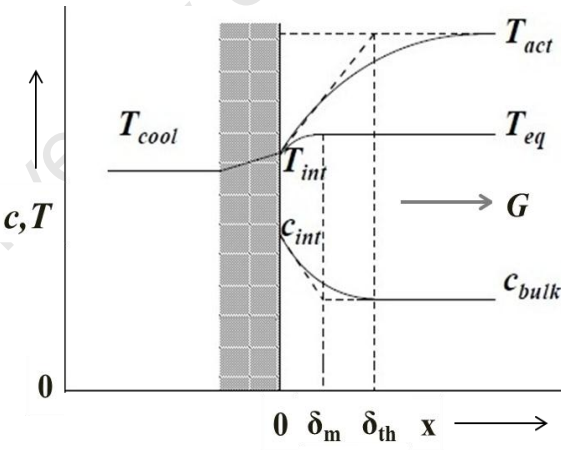

Figure 8: Temperature and concentration profile (Myerson, 2000, p.8)

The actual (real) temperature T_{act} is always above the equilibrium temperature except at the interface where the actual temperature can be lower. The actual temperature at the interface depends on the specific process conditions (Myerson, 2002).

2.2.2 Diffusion boundary layer

The diffusion boundary layer is defined as a liquid region close (above) to the solid–liquid interface through which diffusion occurs (Mullin, 2001; Wang et al., 2003). The diffusion boundary layer can be thermal δ_{th} or mass layer δ_{m} as shown in Figure 8 above. In this region, the temperature and concentration is not the same as that in the bulk due to heat and mass transfer interactions. The thickness of the diffusion boundary layer can be related to the effective impurity distribution coefficient and affects the rate of crystal growth (Myerson, 2002) . The processes in the boundary layer may influence interface morphology and its stability (Sato et al., 2001). The thickness of the boundary layer is given by the diffusion distance:

$$\mathrm{l_D} = \frac{\mathrm{D}}{v} \qquad \text{Equation 2-3}$$

where D ($cm^2 s^{-1}$) is the diffusivity and v ($cm\, s^{-1}$) is the growth rate of the advancing crystal. Generally, the thermal boundary layer is thicker than the mass boundary layer (Jackson, 2004).

2.2.3 Constitutional supercooling

When the solutes are rejected from a growing crystal, the solute in the growing front increases the concentration. To this concentration profile, a profile of equilibrium temperature corresponds resulting from the phase diagram. When the real temperature of the solution at the solid–liquid interface is locally lower than the equilibrium temperature, it leads to an additional supercooling in front of the interface. This phenomenon is called constitutional supercooling (Myerson, 2002).

The existence of constitutional supercooling, shown by the shaded area in Figure 9, results in unstable conditions for crystal growth (Petzold & Aquilera, 2009) and leads to an inherent tendency for irregular growth in many instances which results in impurity inclusions of the crystalline material (Van't Land, 2005).

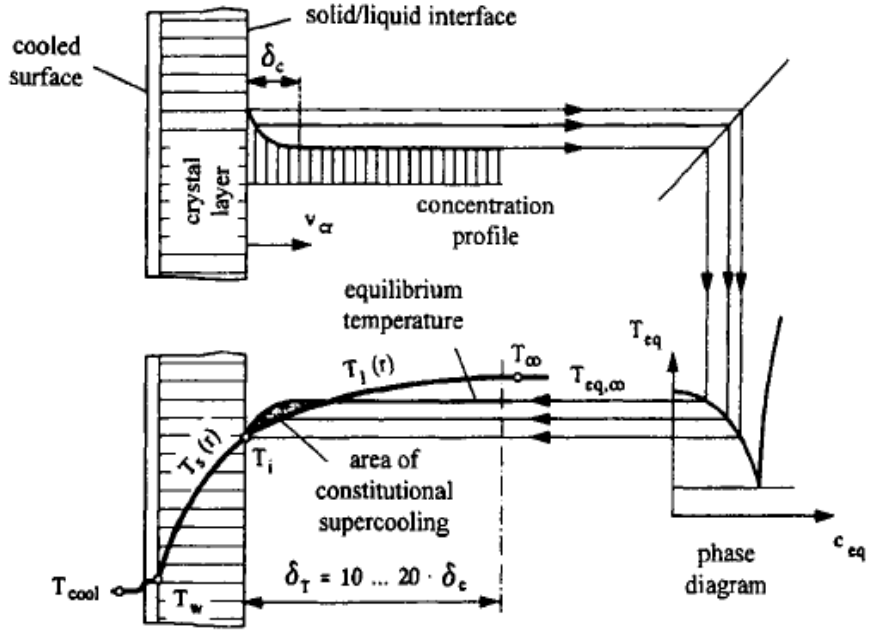

Figure 9: Constitution supercooling (Myerson, 2002, p.165)

To quantify the conditions at which no constitutional supercooling occurs, the solution temperature at the solid–liquid interface must be greater than or equal to the equilibrium temperature (Myerson, 2002).

2.2.4 Ice crystallization

Before the ice crystallization process occurs at the equilibrium freezing point, a significant energy barrier must be overcome by generating a large driving force. This is demonstrated by a process called supercooling or undercooling where sensible heat is continuously withdrawn without resulting in a phase change. The degree of supercooling dictates the onset of ice nucleation (Petzold & Aquilera, 2009).

Once stable ice nuclei are formed, crystal growth is possible by the addition of molecules to the interface. The rate of crystal growth v (mm/s), is a function of supercooling, ΔT_s $(°C)$, reached by the system according to the expression:

$$v = \beta(\Delta T_s)^n \qquad \text{Equation 2-4}$$

where β $(mm/°C.s)$ and n are experimental constants.

Figure 10 shows the temperature–time profile during the freezing process of pure water and aqueous solution (Akyurt et al., 2002). From **A** to **B** or **B'**, the pure water and solution is undercooled. Crystallization of ice for pure water is initiated at **B** and for a solution at **B'** after the metastable zone width of the system is exceeded. The subsequent release of latent heat of crystallization, which at this stage is faster than the heat removed from the system, results in a temperature jump to **C** (0^oC) or **C'**(T_f).

In pure water, crystal growth process is from **C** to **D**. The temperature only drops from **D** to **E** after crystallization is complete as sensible heat of ice is removed.

In aqueous solutions with concentration less than eutectic composition, **C'C*** defines a period in which a freeze process occurs where ice is formed as water freezes out from a solution. At **C***, a salt will crystallize resulting in a slight temperature jump due to the release of heat of crystallization The freezing temperature of the solution is maintained up to **D'** and during this period both the ice and the salt form simultaneously. The temperature only drops from point **D**' to **E'** after crystallization of both the ice and the salt is complete.

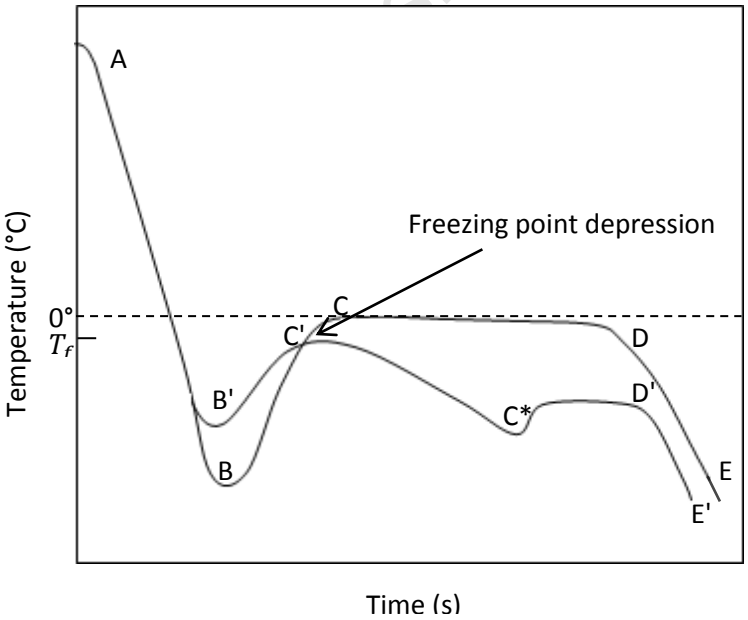

Figure 10: Process of crystallization ice from pure water and solution (Adapted from Akyurt et al., 2002, p.1777)

2.2.4.1 Morphology

Morphology relates to the physical form and structure of a material and it is determined by internal and external factors i.e. growth parameters (Sato et al., 2001). Ice morphology affects the efficiency of the separation between ice crystals and the solutes. Morphology of ice grown from supercooled water can be disk, dense branching, dendritic, needled branch or platelet. When grown from a solution, the morphology can be hexagonal units, dendritic or spherulites (Petzold & Aquilera, 2009). Figure 11 shows the morphology of snow crystals at various supersaturations and temperatures (Libbrecht, 2005).

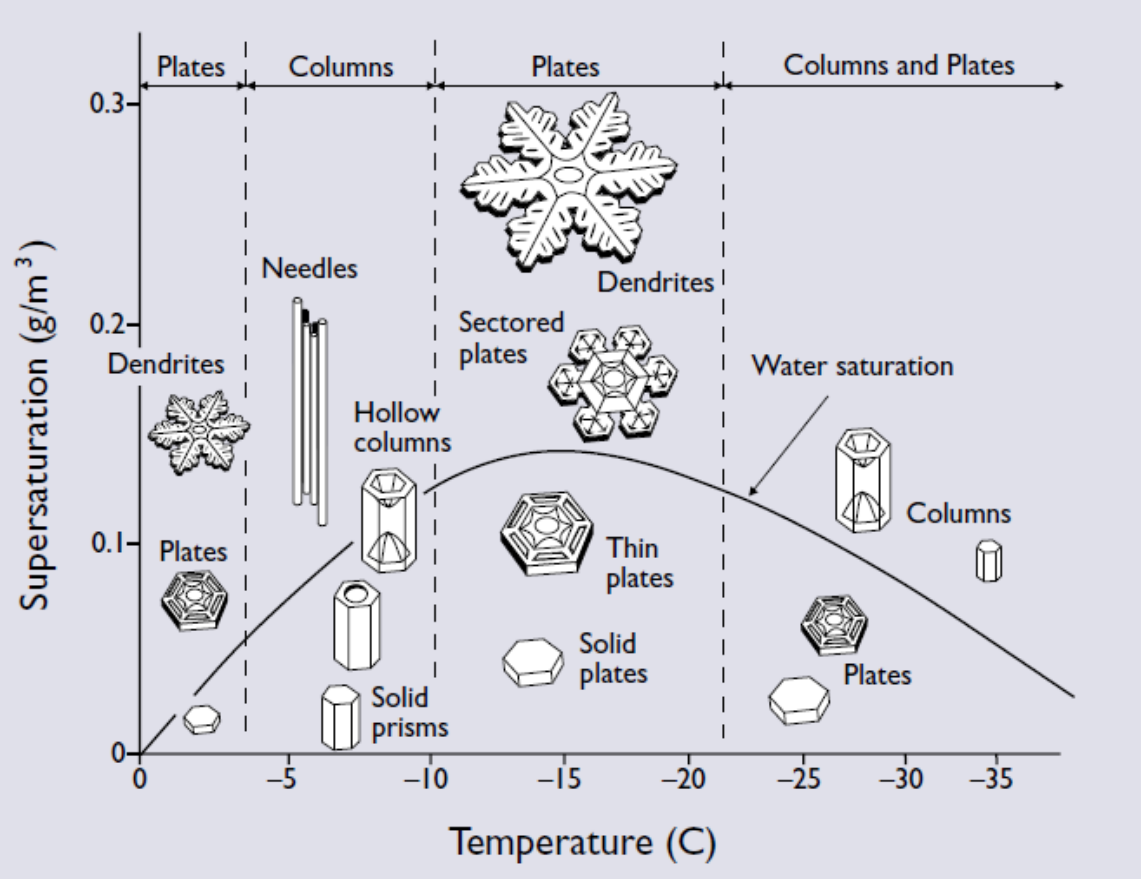

Figure 11: The snow crystal morphology (Libbrecht, 2005, p.860)

Dendrites commonly grow under transport-limited conditions, where the transport of heat or species dictates the behaviour of the solid–liquid interface. For example, in pure systems, latent heat of crystallization from the advancing crystal–melt interface is the controlling factor for dendritic growth. However, in solutions, propagation of dendrites is often controlled by diffusion of solutes since it is generally slower than thermal diffusion (Glicksmann & Lupulescu, 2004). Increasing supercooling causes the growth of dendrites due to increased constitutional supercooling (Sei et al., 2002).

The final ice crystal morphology depends on the conditions under which the crystal was formed and grown as well as the rate of crystal growth and solution temperature (Petzold & Aquilera, 2009).

Shibkov and co-workers (2003) developed a morphology diagram for ice-water system for supercooling range of 0.1 °C <ΔT <30 °C. In their studies, they observed that there were specific supercooling ranges in which two or three different morphological phases may simultaneously coexist. Figure 12 shows the morphology diagram of ice growing in pure water (Shibkov et al., 2003).

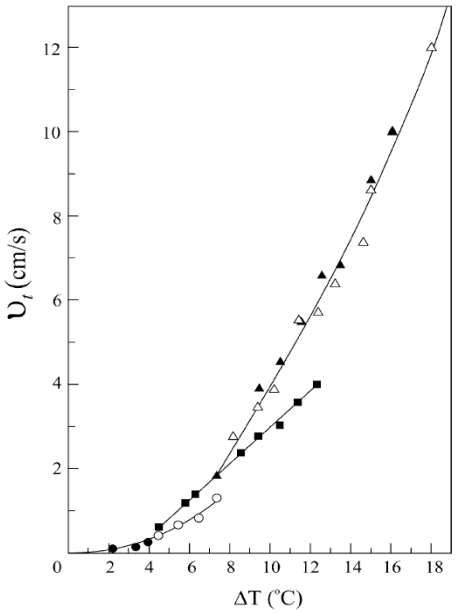

Figure 12: Morphology diagram of nonequilibrium growth patterns in $\boldsymbol{v_t} - \Delta \boldsymbol{T}$ phase space: (●) dendrite; (○) stable needle-like crystal; (■) fractal needled branch; (▲) compact needled branch; (Δ) platelet. (Shibkov et al., 2003, p.73)

2.2.4.2 Impurity incorporation in ice crystals

Crystals can contain foreign impurities. These may be solid, liquid or gas (Mullin, 2001) and can be incorporated by entrainment, isormophous substitution or through inclusion. Impurities tend to enter the crystal lattice because of chemical and structural similarities of the impurities with the crystal. Impurities can also enter the crystal and segregate along the defects in the lattice.

However, mechanisms by which the impurities can be incorporated in ice crystals are either by liquid entrainment or solid/liquid inclusion. Isormophous substitution is unlikely to occur because of molecular differences between the water molecule and that of the salts as can be seen between water (H_2O) and sulphate (SO_4^{2-}) in Figure 13 illustrated by Venter (2011). Isomorphism is when crystals of different species have similar structure and same type of bonding and unit-cell dimensions. These macroscopically appear identical (Myerson, 2002) like sulphate and selenite molecules. Because of their similarities, isormophous substitution can occur during crystallization. Liquid entrainment is when the mother liquor becomes trapped between aggregated crystals and these can easily be left behind after filtration.

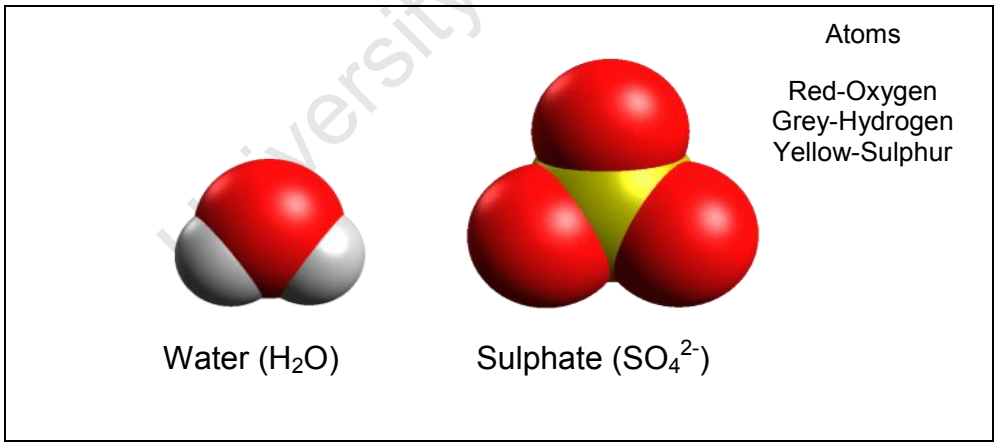

Figure 13: 3-D presentation of water molecule to scale with the sulphate molecule (Venter, 2011; used with permission).

Inclusions are pockets of impurities (Mullin, 2001) and these are generally distributed in a random array in the crystalline matrix though sometimes they do appear in regular patterns (Myerson, 2002)**.** Figure 14 shows some regular channels formed in ice grown from brackish water (Luo et al., 2010). Inclusions can be in the form of random clusters or sheets of small bubbles or parallel channels. They generally account for the largest in impurity levels in a crystal (Bennett, 2000). In order for an inclusion to form, the crystal–liquid interface must break up and grow in an unstable manner. The formation of inclusions also appears to be related to crystal/solution parameters affecting heat and mass transfer to the growing crystal. Factors such as rapid crystal growth and uneven levels of supersaturation are known to be related to the formation of inclusions (Myerson, 2002)**.** Impurity inclusions can be removed effectively by a sweating process where a sweated melt containing a high concentration of impurities is drained off (Mersmann, 2001). A sweating process is a partial melting of crystals by means of warm gas or heating of the cooled surface closely up to the melting point of the pure component (Myerson, 2002).

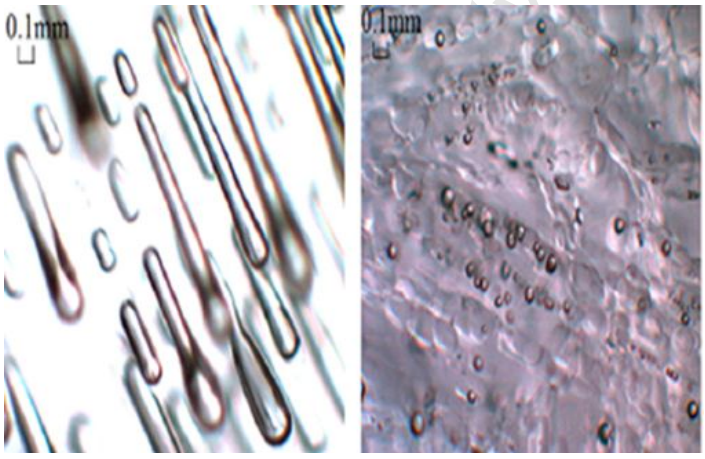

Figure 14: Brine inclusion through channels formed in ice grown from brackish water (Luo et al., 2010, p.237)

2.3 Heat and mass transfer

Crystallization is essentially a coupled heat and mass transfer process. Depending on the type of crystallization, either one of them is a dominating process. Heat transfer is due to a temperature difference. Therefore, it occurs when there are inhomogeneities in temperature distribution within a material or between the material and the surrounding.

There are three modes of energy transfer, i.e. conduction, convection and radiation. All heat-transfer processes involve one or more of these modes. The transfer of energy by conduction is accomplished by molecular interactions or by 'free' electrons of a substance(s). The heat transfer by molecules is present, to some degree in all systems in which temperature gradients exist and in which molecules of a solid, liquid or gas are present. Heat transfer by electrons usually occurs in metallic solids. Heat transfer by convection involves the energy exchange between a surface and an adjacent fluid (Welty et al., 2007).

The heat transfer by conduction can be described by Fourier's law where the heat transfer rate, q (W) per unit area, A (cm^2), is proportional to the temperature gradient, $\frac{dT}{dx}$ $(°C/cm)$, along the direction of heat flow:

$$\frac{q}{A} = k\frac{dT}{dx} \qquad \text{Equation 2-5}$$

k $(W/cm\ °C)$ is the thermal conductivity of the substance

An expression of the overall effect of convection is defined by using Newton's law on cooling:

$$q = hA\Delta T \qquad \text{Equation 2-6}$$

Here the heat transfer rate is related to the overall temperature difference ΔT between the wall and the fluid and the surface area, A. h is the convection heat transfer coefficient in $W/cm^2\,°C$ (Holman, 1981).

Mass transfer involves the transfer of species in a mixture due to a concentration difference. It can be expressed as:

$$N_i = k(C_i - C_b)N_i \qquad \text{Equation 2-7}$$

$N_i\,(mol/cm^2\,sec.)$ is the flux, $k\,(cm/sec.)$ is the mass transfer coefficient and $C_i - C_b$ (mol/l) the concentration difference between the interface and the bulk solution

2.3.1 Heat and mass transport equations for ice crystallization

Details of the following derivations and relations of heat and mass transport based on irreversible thermodynamics and the Onsager relations have been extensively explored by Kjelstrup and Bedeaux (2008). All transport equations are governed in principle by the second law of thermodynamics. Unlike the first law of thermodynamics, which gives the rate of a process, the second law gives the direction instead (Kjelstrup & Bedeaux, 2008) . In non-equilibrium thermodynamics, the second law is assumed to remain valid locally (Genceli et al., 2009).

Below is the summary of relevant equations for ice crystallization in water and aqueous solutions based on irreversible thermodynamics and Onsager relations. The mass flux (J) during ice crystallization is calculated from the ice growth rate (v_{ice}) using:

$$J^l = \rho_{ice} v_{ice} \qquad \text{Equation 2-8}$$

where J^l $(mol/m^2 s)$, is the mass flux on the liquid side, $\rho_{ice}\,(kg/m^{-3})$ is the density of the ice and $v_{ice}\,(m/s)$ is the growth rate of the ice.

The heat flux into the liquid side can be determined by Fourier's law for heat transport assuming the conductivity on the liquid side is the same, giving:

$$J_q^{\prime,l} = -\lambda_{ice-aq}\frac{dT}{dx} \qquad \text{Equation 2-9}$$

Where $J_q^{\prime,l}$ $(J/m^2 s)$, is the heat flux into the liquid side, λ_{ice-aq} $(W/m.K)$ is the thermal conductivity of ice and T is the temperature in K.

Equation 2-9 assumes the conductivity on the liquid side is the same. It gives a continuous flux profile away from the ice surface.

According to Onsager relations (Kjelstrup & Bedeaux, 2008), the interface resistivities to heat transfer where $R_{qq}^{i,s} = R_{qq}^{i,l}$, the heat transfer coefficient ratio,$q^{*i,l}$, for the liquid side can be evaluated and defined as:

$$q^{*i,l} \equiv \left(\frac{J_q^{i,l}}{J}\right)_{T^s=T^l} = -\frac{R_{q,u}^{i,l}}{R_{qq}^{i,l}} \qquad \text{Equation 2-10}$$

where $R_{qq}^{i,s}$ is the heat transfer resistivities of the surface to the liquid side and $R_{qq}^{i,l}$ is the heat transfer resistivities of the surface to the liquid side in $m^2\, s/J.K$, $R_{q,u}^{i,l}$ is the film resistivity of the surface to the liquid side in $m^2 s/mol.K$ and $q^{*i,l}$ is the heat of transfer coefficient ratio to the liquid side of the surface in J/mol .

2.4 Method employed in this study: The Colour Schlieren technique

The growth history and defect structure of a crystal is a function of the time dependant spatial distribution of convection patterns, temperature and concentration profiles. Therefore, an understanding of crystal growth mechanisms and factors that affect the purity of crystals requires knowledge of spatial distribution of parameters that affect growth. Non-intrusive techniques are a useful and fruitful experimental approach towards such studies (Shlichta & Verma, 2008). Examples of non-intrusive techniques are imaging techniques such as Interferometry, Schlieren and Shadowgraph (Settles, 2001; Srivastava et al., 2004; Shlichta & Verma, 2008; Hargather & Settles, 2012) and the use of thermochromatic liquid crystals (TLC) for temperature and heat transfer measurements (Stasiek & Kowalewsk, 2002; Yang et al., 2007).

It is generally recognized that optical techniques are powerful tools to investigate heat and mass transfer in transparent fluids (Ambrosini et al., 2008). Since they are non-intrusive, they enable the analysis of test regions to be performed in the absence of instrument probes. It is practically impossible to spatially map the temperature and concentration profiles with traditional probes. Also, the presence of probes in the test media could disturb the processes under investigation.

Colour Schlieren is an optical technique that measures changes in the refractive index of the solution caused by variations in solution density, due to differences in either concentration or temperature. Therefore, Colour Schlieren gives the capability to measure temperature/concentration by mapping the gradient variations of the refractive index in the solution. This technique was used for most of the experiments in this work.

2.4.1 Principle operation of the Colour Schlieren technique

The Colour Schlieren technique is an optical imaging technique. Image formation in a Schlieren system is caused by the deflection of the light beam in a variable test field towards a region of higher refractive index. The Colour Schlieren images are representative of the changes in refractive index of the medium along the passage of light. The changes in the refractive index measured are the average gradient over the path of the light beam. The images carry information related to the first derivative of the refractive index of a transparent material which is related to temperature and concentration.

Quantitative information for temperature and concentration gradients can be obtained from an adequately designed magnitude-indicating Colour Schlieren system. A detailed description has been done by Hargather and Settles (2012).

The setup of a Colour Schlieren consists of a white light source connected to a pinhole with fibre-optical cable for obtaining a point light source. The pinhole is placed at the focal length of the first lens to collimate the light going through the test cell where crystallization occurs. The test cell is placed between the first and the second lens which focuses the light onto a colour filter. The colour filter is positioned in front of the second lens at its focus. The optical data is recorded by a camera which is connected to a computer acquisition system.

The colour changes from the filter represent both the magnitude and the direction of an encountered density gradient in test media in the test cell.

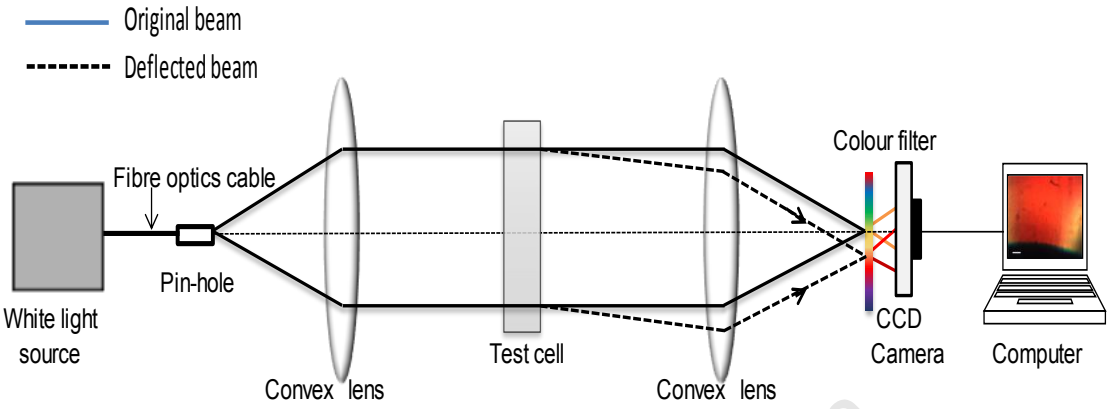

Figure 15: Colour Schlieren deflectometry setup (Adapted from Gupta et al., 2010, p.818)

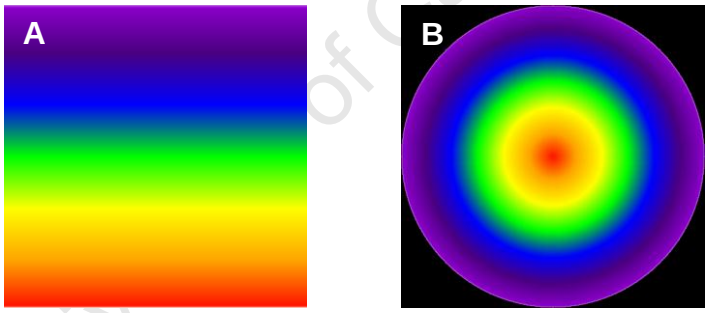

Figure 16: Colour filters; A – 1-D filter; B – 2-D axisymmetric filter (Seithia et al., 2010)

2.5 Review

2.5.1 Ice growth processes and quality of ice crystals

Crystallization is generally done to produce high-purity products, hence it is important that crystals are grown in such a way that impurities which are part of the mother liquor are not carried out with the crystalline particles (Bennett, 2000). A number of experiments on factors affecting the purity of ice in ice crystallization processes have been carried out.

Reddy and co-workers (2009) ran EFC experiments of a Na_2SO_4-H_2O binary system to investigate factors affecting separation. It was found that introducing agitation in a separation vessel increased the purity of ice by 75% and, with the addition of wash cycles, the purity was increased by approximately 90%. The introduction of agitation changes the dynamics of heat and mass transport in the system.

Tao and Liqiu (2007) investigated the study on factors affecting ice crystal purity during a freeze concentration process for urine treatment. The results showed that more than 99% of inorganic salts can be removed with appropriate cooling rate, seeding, re-crystallization process and crystallization time (Tao & Liqiu, 2007).

Chen and co-workers (1998) investigated the effects of ice growth rate and solute concentration on solute inclusion in ice under constant flow conditions. The trends showed that solute inclusion in ice formed from sucrose on a sub-cooled surface increased with increasing growth rate and bulk concentration (Chen et al., 1998) .

Terwilliger and Dizio (1970) did some fundamental studies on salt rejection and entrainment phenomena. They examined salt redistribution processes that occur during the freezing of a NaCl solution and the factors responsible for salt rejection. It was observed that solute boundary layer thickness varied inversely with the freezing rate and ranged from 60-600μ for freezing rates ranging from 4-45μ/sec. Two parameters found to control the redistribution process were; the liquid phase interface concentration which is controlled by constitutional supercooling and the thermal driving force imposed on the system to initiate and maintain freezing (Terwilliger & Dizio, 1970) .

Grange and co-workers (1976) studied diffusion of heat and solute during freezing of salt solutions using Mark-Zander interferometry. It was found that at the crystalline interface, concentration is not constant but increases with time due to increased solute rejection. They also postulated that mechanisms controlling solute rejection could change during crystallization in a finite region.

Myerson and Kirwan (1977) studied the trapping process of impurities during dendritic crystal growth from an aqueous solution. They showed that the process of impurity trapping depends on the crystal growth rate, interfacial temperature gradient and the bulk liquid composition.

2.5.1 Ice growth rate

Huige (1972) studied the growth of ice from still water and aqueous solution using distilled water and various concentrations of aqueous dextrose solution. He found that for still water, the growth rate of ice could be correlated by:

$$v_{ice} = 0.03\ (\Delta T_b)^{2.22} \qquad \text{Equation 2-11}$$

where v_{ice} (cm/s) is the ice growth rate, 0.03 is a constant in $cm/°Cs$ and ΔT_b is the bath supercooling varied between 0.8 and 4 °C.

However, studies of Kallungal and Barduhn (1977) for ice growth rate in quiescent pure for subcooling of 0.1 and 1 °C were found to fit the relation:

$$v_{ice} = 0.0118\ (\Delta T)^{2.17} \qquad \text{Equation 2-12}$$

where v_{ice} (cm/s) is the growth rate of ice, 0.0118 is a constant in $cm/°C\,s$ and ΔT is the bath supercooling.

Barduhn and Huang (1987) investigated why ice grows faster in dilute sodium chloride solutions of less than 1 wt% than in fresh-water under the same degree of

supercooling. They solved equations of Navier-Stokes law, continuity, and diffusion by Fick's law and related the growth rate with respect to the radius of the curvature of the nose of the parabolic ice crystal. The ice growth rate equation predicted a sharp increase in growth rate as the solution increased in salt content from 0 to a few tenths of 1 wt%. They concluded that the anomalous growth rate was caused by convections caused by gradients of both temperature and concentration (Barduhn & Huang, 1987).

2.5.2 Heat and mass transfer effects in ice crystallization

Crystallization is a dynamic process in which molecules or ions diffuse and absorb on the crystal surface simultaneously during growth. Usually, in crystallization calculations all the heat of crystallization during growth is transferred to the cold side (Mersmann, 2001; Pronk, 2006).

Ratkje and Fresland (1995) presented a theoretical study of ice growth from a subcooled falling film of aqueous solution. Coupled heat and mass flux equations from irreversible thermodynamics were used to describe the ice growth under approximately stationary conditions. In their work, irreversible thermodynamics were used to predict the effect of temperature gradients on the growth rate of ice crystals. Equation 2-13 presents an irreversible thermodynamics (IT) model that was developed Ratkje and Flesland (1995) and was valid for one dimension transport problems. Figure 17 is a diagram showing transport of heat J_q, water and solute(s), represented as the velocities relative to the surface, v_{H2O}^{ice} and v_s^{ice} as well as the ice growth rate v_{ice}, temperature and concentration profiles (Ratkje & Flesland, 1995).

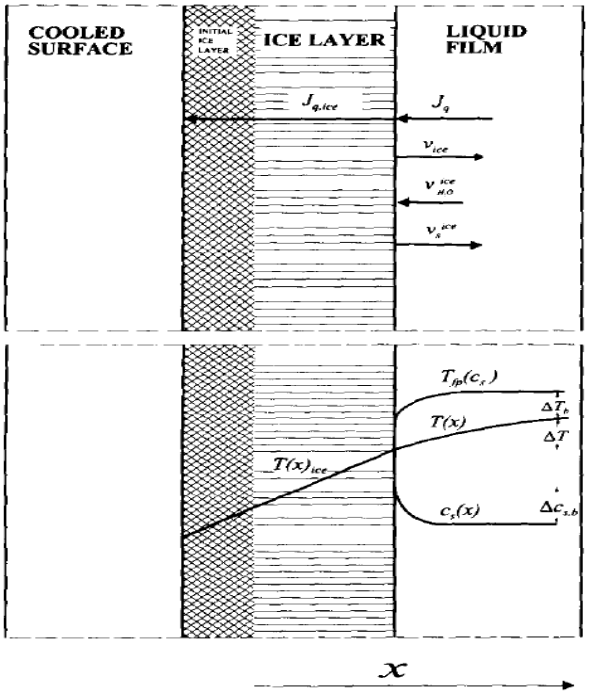

Figure 17: The IT model system (Ratkje & Flesland, 1995, p.556)

$$v_{ice}^{wall} = \left[1 + \frac{1}{C_{H2O}(V_{ice} - V_{H2O})}\right]\left(\frac{DC_{H2O}}{RT}\right)\left(\frac{\lambda}{T}\frac{dT}{dx} - \frac{RT}{C_{H2O}}\frac{dC_s}{dx}\right) \quad \text{Equation 2-13}$$

However, Chen and co-workers (1997) compared the IT models with their model described by Equation 2-14. Unlike the IT model which was developed from irreversible thermodynamics, this model was obtained by applying the conventional heat and mass transfer thermodynamics (Chen et al., 1997).

$$v_{ice}^{wall} = \frac{1}{C_{H2O}}\left[1 + \frac{1}{C_{H2O}(V_{ice} - V_{H2O})}\right]\left[\frac{k_{ice}}{\lambda}\left(\frac{dT}{dx}\right)_{ice} - \frac{k_{H2O}}{\lambda}\left(\frac{dT}{dx}\right)_{H2O} - \frac{D_{s,H2O}C_{p,s}T}{\lambda}\left(\frac{dC_s}{dx}\right)_{H2O} - \frac{D_{H2O,s}C_pT}{\lambda}\left(\frac{dC_{H2O}}{dx}\right)_s\right] \quad \text{Equation 2-14}$$

where;

v= Ice growth rate (m/s)

V= Volume (m^3)

C= Concentration (mol/m^3)

R= Molar gas constant $(J/mol.K)$

D= Diffusion coefficient (m^3/s)

T= Temperature (K)

λ= Enthalpy of freezing (J/mol) K= Heat conductivity $(W.m.K)$

C_p= Specific heat capacity $(J/mol.K)$ x= Space coordinate (m)

S= Solute

The two models predicted opposite results. Chen argued that the IT model involved heat flux equations that did not contain an energy balance and therefore did not take into account of the temperature gradient on the ice side of the ice –liquid interface. However, it was elaborated by Kjelstrup and Bedeaux (2008) that the theory of irreversible thermodynamics with the use of Onsager relations prescribes that coefficients, like thermal conductivity, can depend on temperature, but not on the gradient of the temperature. Therefore, the temperature gradient on the ice side of the ice-liquid interface which was not taken into account did not affect the outcome of their results.

Most recently, Geneceli and co-workers (2009) used heat and mass transport equations based on irreversible thermodynamics coupled with the use of Onsager equations which predicted a temperature jump in crystallization. They argued that the equation derived from Equation 2-10 shows that the assumption of zero-cross coefficients violates laws of thermodynamics (Genceli et al., 2009).

$$q^{*i,s} - q^{*i,l} = \Delta H_{cryst} \qquad \text{Equation 2-15}$$

where $q^{*i,s}$ and $q^{*i,l}$ (J/mol) are the heat transfer coefficient ratios to the solid side of the surface and to the liquid side of the surface respectively.

From this, the fraction of the enthalpy carried from the cooled surface through the crystal into the liquid was defined with a parameter k:

$$\mathrm{k} = \frac{q^{*i,l}}{\Delta H_{cryst}} \qquad \text{Equation 2-16}$$

Using the above equations, Genceli and co-workers (2009) showed that heat of crystallization is transferred both to the solid and the liquid side during crystallization. This would then result in a temperature jump between the two phases of the solid–liquid interface. For the case of epsomite, at the growth rate of 2.33 x 10^{-3} $mol\ m^{-2}s^{-1}$, about 20-30% of heat of crystallization was calculated to be transferred back to the liquid side and the remainder of 70-80% to the solid side. This is in accordance with predictions of irreversible thermodynamics (Genceli et al., 2009).

2.6 Temperature/Concentration-Refractive index relationship of H_2O and H_2O-$MgSO_4$ system

The change in refractive index of solutions as a function of concentration and temperature is an essential characteristic for several optical measuring techniques (Angnes et al., 2004; Chen et al., 2008). In Colour Schlieren deflectometry, the measured change in refractive index is related to parameters like density, temperature and concentration.

In this study, a pure water system and an aqueous magnesium sulphate solution were investigated. Therefore the formulation of the refractive index of the two systems was of interest.

Schiebener and co-workers (1990) published a formulation for refractive index of water and was adopted by the International Association for the Properties of Water and Steam (Schiebener et al., 1990). Harvey and co-workers (1998) presented a revised version which was more accurate and is represented by the following equation:

$$\frac{n^2-1}{n^2+2}\left(1/\bar{\rho}\right) = a_0 + a_1\bar{\rho} + a_2\bar{T} + a_3\lambda^{-2}\bar{T} + {a_4}/{\rho^{-2}} + \frac{a_5}{\lambda^{-2}-\lambda_{UV}^{-2}} + \frac{a_6}{\lambda^{-2}-\lambda_{IR}^{-2}} + a_7\rho^{-2} \qquad \text{Equation 2-17}$$

where n is the refractive index of water

The coefficients a_0a-a_7 and the constants λ_{UV} and λ_{IR} are given in Appendix A2 .The formula is valid between temperatures of -12 to 500 °C (Harvey et al., 1998).

The formulation of the refractive index of inorganic solutions has not been extensively researched. Most of the refractive index data available represents the change of refractive index with concentration at constant temperature. However, Leyendenkkers and Hunter (1977) deduced a formula for refractive index as a function of concentration at various temperatures for different inorganic solutions. They applied the Eisnberg Refractive Index (Equation 2-18) and Tammann-Tait-Gibson (Equation 2-19). The formulas allow calculation of the refractive index and concentration at different temperatures (Leyendekkers & Hunter, 1977).

$$f(n) = A(\frac{1}{\varphi_w})^B \exp(-Ct) + \Delta f(n) \qquad \text{Equation 2-18}$$

$$f(n) = [\frac{2f(n)+1}{1-f(n)}]^{0.5} \qquad \text{Equation 2-19}$$

where $f(n)$ is a function of refractive index and is equal to $\frac{n^2-1}{n^2+2}$ and t is the temperature in °C.

Details of the formulation are available in the reference. The major limitation of the formula, however, is the range of validity, which is between the temperatures 0 and 40 °C.

2.7 Context and scope

During Eutectic Freeze Crystallization, three components are present i.e. ice, salt and the solution at eutectic composition. Separation of the ice from the salt can easily be achieved by exploiting the density difference between ice and salt. With typical density values of less than 0.9 kg/l, ice floats in the mother liquor of density of 1.0-1.2 kg/l, and the salt of density of 1.2-1.7 kg/l, sinks to the bottom of the crystallizer. In order to form the ice and the salt crystals at the same time, the system must be operated under eutectic conditions.

The focus of this project is on the heat and mass transfer effects in ice growth processes. For this reason, the planned experiments were not necessarily operated under eutectic conditions where salt would form as well. Even though the process of separation between the ice and the salt affects the purity of ice, studies were focused on the interaction of the ice with the surrounding bulk solution, especially on the solid–liquid interface region.

In this work, two systems were considered. First the pure water system and then aqueous salt solution systems of magnesium sulphate and sodium nitrate. In the case of salt solutions, only binary systems were considered. This is because it is easier to carry out the studies with a binary system than a multi-component system.

This research looked at the fundamental aspects of heat and mass transfer and its effects on local supersaturation, crystal growth rate and morphology. Experiments carried out were layer based crystallization where ice was grown in a cooled surface in a cell crystallizer without agitation. The results and findings can be applied to other melt crystallization process. Since ice crystallization from water and dilute aqueous solutions is a heat transfer controlled process (Myerson, 2002), heat transfer measurements may result in better understanding of the ice formation mechanisms (Meewisse & Ferreire, 2003).

2.8 Hypothesis

- Heat and mass diffusion are the principle processes responsible for crystal growth. The combined effect of heat and mass diffusion on local supersaturation affects crystal growth and morphology. A high supersaturation results in a high growth rate and leads to dendritic ice formation.

Figure 18 shows the development of the hypothesis. At the beginning of a freezing process, heat is removed from a system. This leads to the creation of temperature gradient and continuous heat removal results in the system being supersaturated. The onset of nucleation and subsequent crystal growth is characterised by generation of heat of crystallization and the rejection of the solute from the growing ice. Part of the heat that is generated is absorbed by the ice while the other diffuses

into the bulk solution thereby creating a temperature gradient at the solid–liquid interface. The solutes that are rejected by the ice diffuse into the bulk solution which also results in an increase in solute concentration at the solid–liquid interface. The diffusion of heat and mass into the bulk forms a diffusion boundary layer where heat and mass transfer interactions occur and affect the local supersaturation. The change in concentration and temperature gradients affects the local supersaturation which in turn affects crystal growth rates and morphology.

Crystal growth rate and morphology affects the quality and purity of ice crystal. The shaded area in the figure represents the area of interest in the current study.

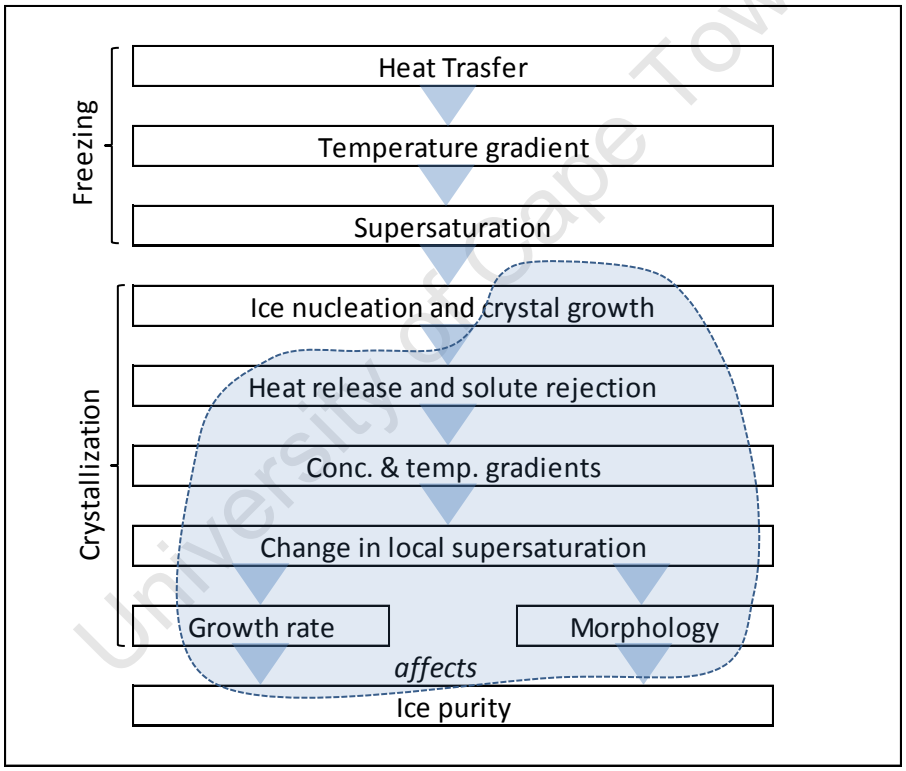

Figure 18: Development of hypothesis

2.9 Objective

The aim of this study is to investigate the factors that affect ice purity during Eutectic Freeze Crystallization by studying the mechanisms that determine the origins of impurities during crystal growth. The objectives are to investigate the heat and mass transfer effects on ice growth processes during growth in water and aqueous solution by:

- measuring concentration and temperature gradients in the solution surrounding growing ice, heat and mass transport in the liquid surrounding the growing ice near the solid–liquid interface;
- studying the effect of local supersaturation variations on crystal growth rate and morphology of ice in water and in aqueous solution.

3 Methodology

The Colour Schlieren deflectometry was used for most of the experiments in this research. This is because it allows the mapping of temperature and concentration profiles of the solution surrounding the growing ice during crystallization.

3.1 Schlieren apparatus

The accuracy of the Schlieren setup depends on the quality of the equipment used and the alignments and positioning of the optical apparatus. For example, the use of achromatic lenses instead of non-achromatic ones limits the effect of chromatic aberration by bringing different wavelengths (from the white light) into focus in the same plane. Chromatic aberration is the formation of coloured fringes in an image due to refraction of light of different wavelengths. The colours red, yellow and blue in Figure 19 show an example of chromatic aberration.

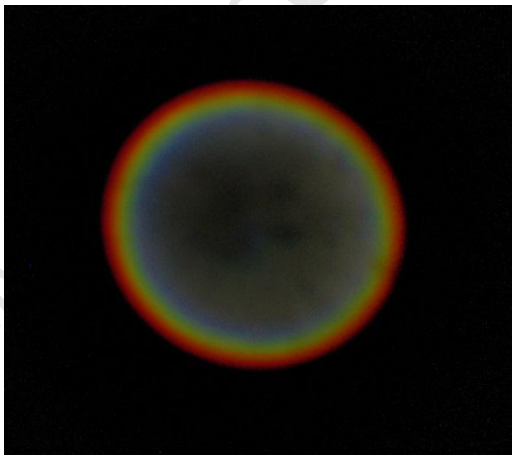

Figure 19: White light through a pinhole showing the effect of chromatic aberration (fringes of colour; red, yellow and blue)

The limitation of the effect of chromatic aberration ensured that the colours recorded in the Schlieren image were purely from refraction of light in the test media due to inhomogeneities.

One of the vital aspects of the Schlieren setup is the positions of the optical equipment. The positions of the test section, the decollimating lens and the digital camera should satisfy the relation:

$$\frac{1}{p}+\frac{1}{q}=\frac{1}{f_2} \qquad \text{Equation 3-1}$$

where p is the distance (mm) between the test cell and the decollimating lens, q is the distance (mm) between the decollimating lens and the camera and f_2 is the focal length (mm) of decollimating lens. The fraction $\frac{q}{p}$ is the magnification of the image that is projected on the lens of the camera (Goldstein, 1996). Figure 20 shows the positioning of the Schlieren apparatus.

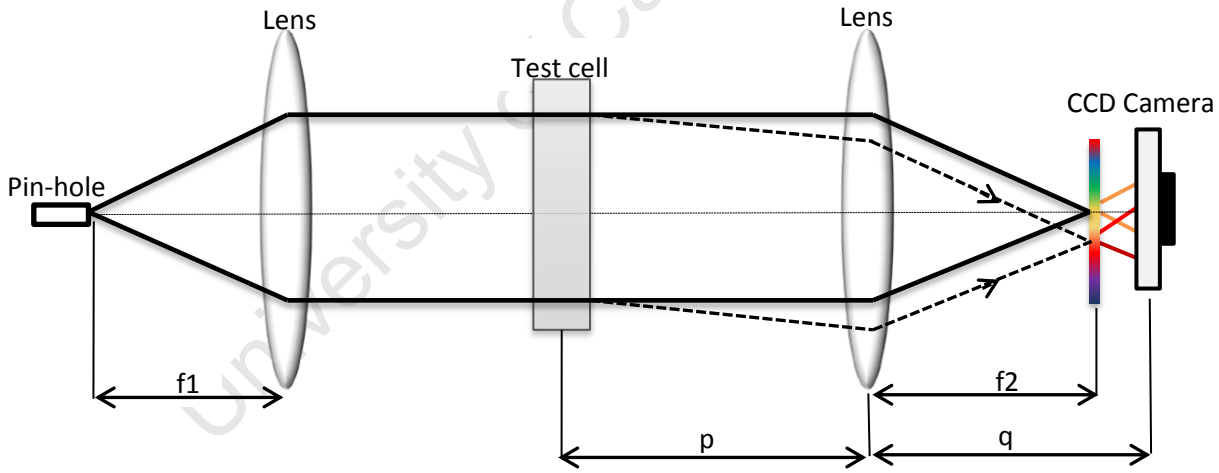

Figure 20: Positioning of Schlieren apparatus

It is important that the locations of the optical equipment satisfies the positions shown in Figure 20 because only when these positions are maintained will the image be in focus without the use of additional objective lenses. It is desired that addition of objective lenses on the camera be avoided as they have a potential of introducing errors due to the introduction of more light deflections before the image is recorded.

It must also be noted that, in a Colour Schlieren setup, there are two types of images present i.e. the real image without colours from the filter and an image with colours. The real image without colour can be captured by partially blocking the light through the colour filter. Figure 21 shows examples of the two images. In order to have a Schlieren image, the images with colours from the colour filter must be superimposed on the real image.

This implies that the deflections taking place at specific locations in the test media would correspond to the colour changes at the same locations in the Schlieren image. This is only possible when the position of the test section, the decollimating lens and the digital camera satisfy the above relations making the Schlieren image in focus.

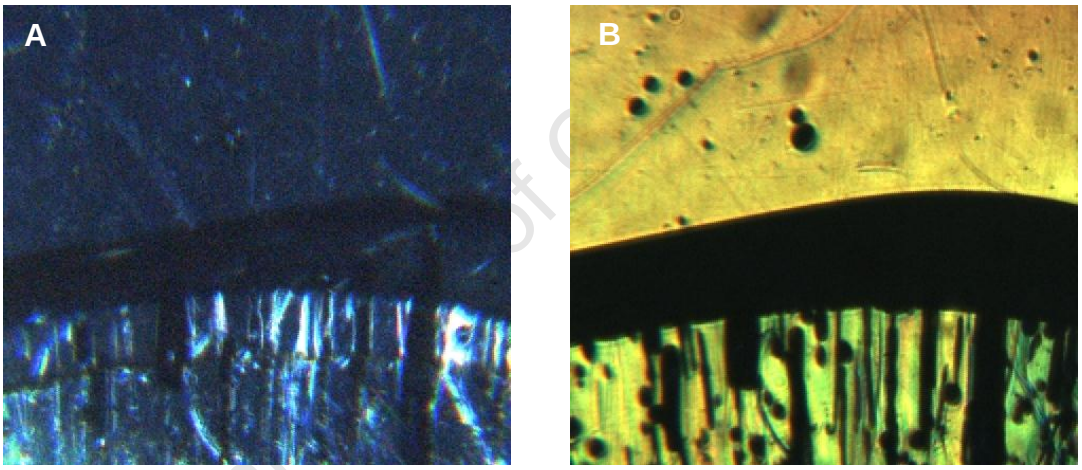

Figure 21: Images of ice in pure water; A – Real image without colour effects; B – Image with colour effects

The distances in the setup were determined in such a way that the light intensity was not compromised but at the same time the image projected on the camera was not too magnified so as to order to record a large section of the test media during the experiment.

3.2 Colour filter generation

A 2-D axisymmetric rainbow filter with radial hue distribution in Figure 22 was designed using Matlab (see Appendix F) and developed on a photographic film. Hue values instead of red-green-blue (rgb) values were used to generate the filter as recommended by Greenberg (1995). This colour scale is used because each colour is uniquely and numerically identified as a hue, independent of dilution by white light (saturation) or its intensity (Greenberg et al., 1995).

To maximise sensitivity, the colours on the filter varied continuously to ensure that light refracted passed through a unique colour based on the refraction angle.

The measuring range (ε_{range}) of the Colour Schlieren is the maximum deflection angle at which linear range of colour indicator (hue) is achieved (Gupta et al., 2010).The measuring range depends on the dimensions of the filter (b_f), size of pinhole (b_s) through which the light passes and the focal length of the decollimating lens (f_2),

$$\varepsilon_{range} = \frac{b_f - b_s}{f_2} \qquad \text{Equation 3-2}$$

where b_f, b_s and f_2 are in mm and ε_{range} is dimentionless.

3.3 Filter calibration

In order to obtain quantitative data, i.e. convert image colour to angle of refraction, the colour filter was calibrated. The refraction angle at any point in the Schlieren image was quantified by finding the displacement distance of the light using colour changes on the image. This was done by capturing the full image of the filter from which a transmissivity function was generated and used for calculation of refractive index.

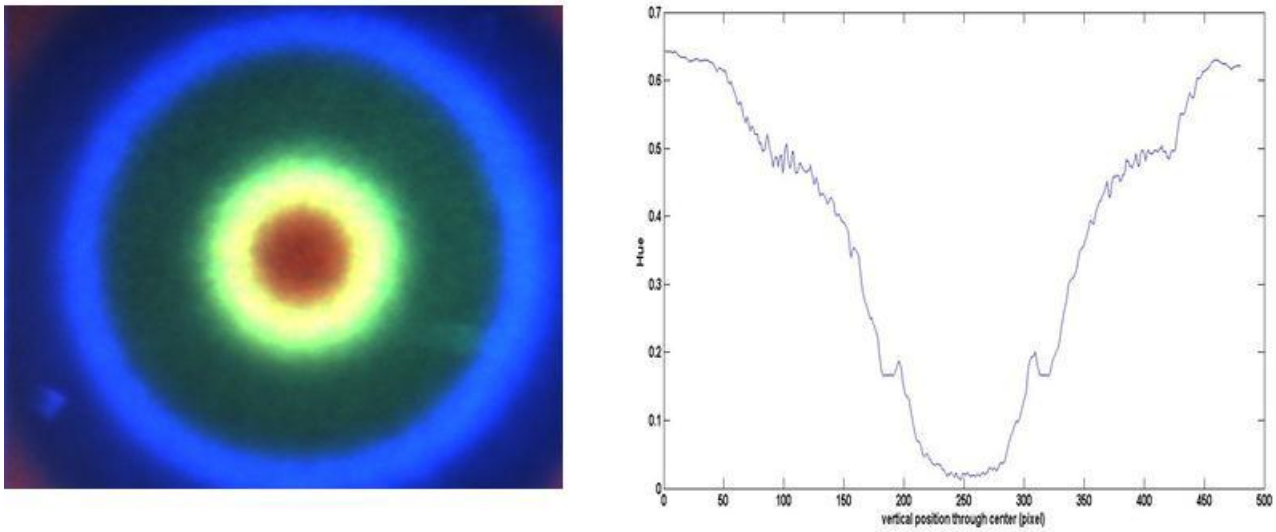

Figure 22: Image of 2-D axisymmetric colour filter and the corresponding transmissivity function

In Figure 23, a curve is fitted into a vertical transmissivity curve and the change in angle with hue.

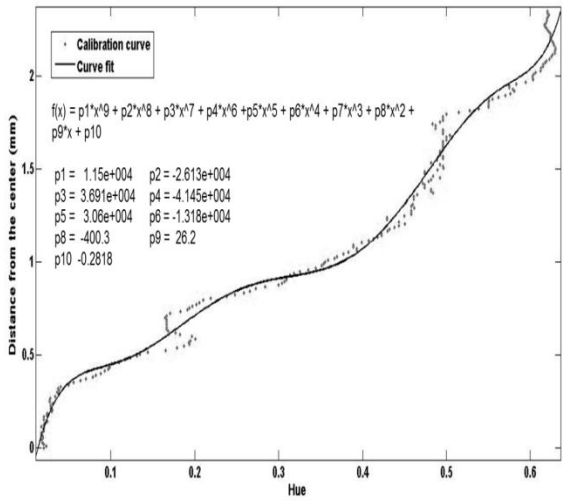

Figure 23: Change in hue with change in distance from the centre of the rainbow filter

3.4 Quantitative analysis

In order to recover quantitative information from a Schlieren image, the deflected angle θ in $radians$ as a function of position in x-y plane (which is normal to the beam) must be determined.

When light is travelling in the z-direction (mm), the ray curvature of the light refracted due to optical inhomogeneities, in proportion to their gradients of refractive index n in the $x-$, $y-$ plane, is given by:

$$\frac{\partial^2 x}{\partial z^2} = \frac{1}{n}\frac{\partial n}{\partial x} \quad , \quad \frac{\partial^2 x}{\partial z^2} = \frac{1}{n}\frac{\partial n}{\partial y} \qquad \text{Equation 3-3}$$

To obtain the components of the angular ray in the respective directions, the equations above are integrated once:

$$\theta_x = \frac{1}{n}\int \frac{\partial n}{\partial x}\partial z \quad , \theta_y = \frac{1}{n}\int \frac{\partial n}{\partial y}\partial z \qquad \text{Equation 3-4}$$

For two-dimensional Schlieren of extent along the optical axis in y direction, this becomes:

$$\theta_y = \frac{L}{n_0}\frac{\partial n}{\partial y} \qquad \text{Equation 3-5}$$

where $L\,(mm)$the length of the test section and n_0 is the refractive index of the ambient air (approximately 1). Therefore,

$$\frac{\partial n}{\partial y} = \frac{\theta_y}{L}$$ Equation 3-6

The beam displacement Δd (mm) of the light beam at the position of the colour filter due to the deflection of light beam passing through the test section by an angle θ_y is given as :

$$\Delta d = f_2 tan\theta_y \approx f_2\theta_y$$ Equation 3-7

Making θ_r the subject of the formula and replacing it into Equation 3-7 gives:

$$\frac{\partial n}{\partial y} = \frac{\Delta d}{f_2 L}$$ Equation 3-8

Equations 3-3 to 3-8 were used to calculate the gradient of the refractive index of the systems under study using image processing and appropriate computational codes. The gradient of the refractive index was related to temperature and concentration gradient using calibration curves. The refractive index gradient was then related to temperature and concentration.

3.5 Experimental setup

3.5.1 Apparatus and instrumentation

The experimental setup is shown in Figure 15. The setup consists of a LED cold white light source (REVOX SLG-50S) connected to a 400 μm pinhole with fiber optical cable for obtaining a point light source. The test cell was placed between the first and the second lens with a distance of 900mm between the test cell and the second lens. The second lens focused the light onto a colour filter of 2.32 mm in radius fabricated on a photographic film. The colour filter was positioned in front of the second lens at its focus. The images were captured using a digital camera with a

resolution of 640x480 pixels located at the conjugate focus of the test section 720 mm in front of the second lens. The camera was connected to a computer acquisition system to record the optical data. The settings of the camera are shown Appendix G. A diaphragm was used to block some of the reflected light in order to improve the accuracy of the set-up.

The optical equipment was placed on translation micro-stages and experiments were carried out in a dark room in order to increase accuracy.

3.6 Solution preparation

De-ionised water, magnesium sulfate ($MgSO_4$) and sodium nitrate ($NaNO_3$) binary salt solutions were used. The concentrations for the magnesium sulfate solutions were formulated as follows:

I. Near eutectic composition
II. Between pure water and eutectic.

The summary of the experiments is shown in Table 3-1. The experiments were designed to study ice growth processes in pure water and in an 8.4 wt% magnesium sulphate solution. The effect of solute concentration on growth rate and morphology were studied by growing ice in an 8.4 wt% and 16.8 wt% of magnesium sulphate solution as well as 8.4 wt% sodium nitrate which was used to compare the effect of different solute species on ice growth rate under the same subcooling.

Table 3-1: Experiment summary

System	Concentration (wt%)		Experiment	No. of Experimental Runs
H_2O			Temperature mapping of water during crystallization Aim: • In-situ measurements of local supersaturation • Study effect of local supersaturation on growth rate and morphology • Quantify heat transferred to the liquid side during dendritic growth	3
$NaNO_3$	8.4		Ice growth rate to determine the effect of solutes on growth rate and morphology	3
$MgSO_4$	8.4	16.4	• Coupled temperature and concentration mapping of solution during crystallization • Ice growth rate to determine the effect of solutes on growth rate and morphology	

3.7 Experimental setup

Ice was crystallized on a sub-cooled plate inside a 10x5x31 mm cell test cell shown in Figure 24. The cell was made of Plexi-glass® (PMMA) and consisted of two compartments separated by 1 mm–thick stainless steel which acted as a heat exchanger. Cooling was achieved by pumping the coolant (Kryo 40) unit using a peristaltic pump (Watson Marlow 505S) into the cooling chamber through the coolant inlet tube which pumped the coolant back to the cooling unit through coolant outlet. Measured amount of water and solutions were injected into the cell using one of the top access tubes of the cell. Temperature readings for the coolant and the solution to get reference points were obtained using k-type thermal couples inserted on the sides of the cell and recorded using a Testo 177-T4 data logger with an accuracy of ±0.3 °C. During cooling, condensation on the walls of the cell was avoided by continuously blowing air on both sides of the cell.

All vibrating equipment such as the pumps and the cooling machine were placed away from the platform where the Schlieren setup was built. In this manner external disturbances and vibrations that would introduce unsteadiness in the flow field of the test cell were avoided.

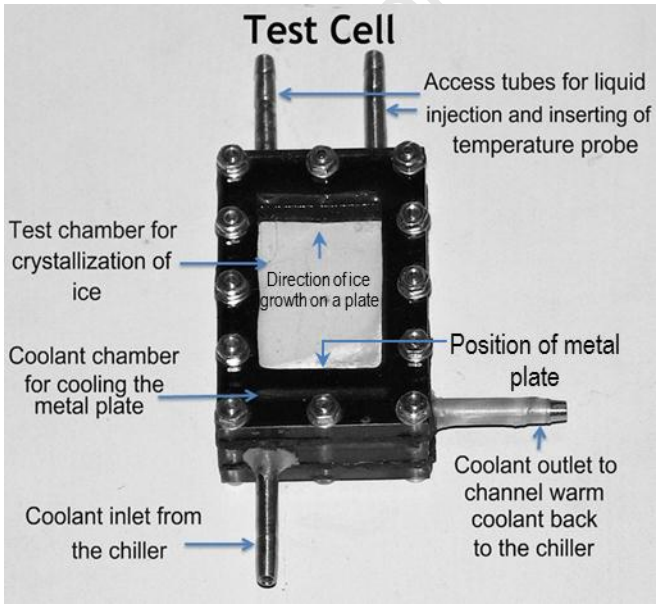

Figure 24: Test Cell

4 Results and discussion

4.1 Thermodynamic modelling of H_2O, H_2O–$MgSO_4$ and H_2O–$NaNO_3$ systems for ice crystallization

In order to understand the behaviour of the systems under study in terms of phase changes, thermodynamic properties were modelled using OLI Analyser® (OLI, 2012). This was particularly important because the results showed the predictions of the temperature at which the phase change from liquid to solid would occur as well as temperatures at which eutectic conditions would be reached during crystallization. As earlier stated (sec. 2.7), it was not desired that the aqueous solutions systems reached eutectic conditions because only the ice was of particular interest.

Figure 25 presents the thermodynamic modelling of the systems which were used in this study. It shows the freezing temperatures of pure water and solutions where ice was expected to form when these temperatures were exceeded. In all the experiments, no salts were formed because ice crystallization was carried out above the respective eutectic points of the systems.

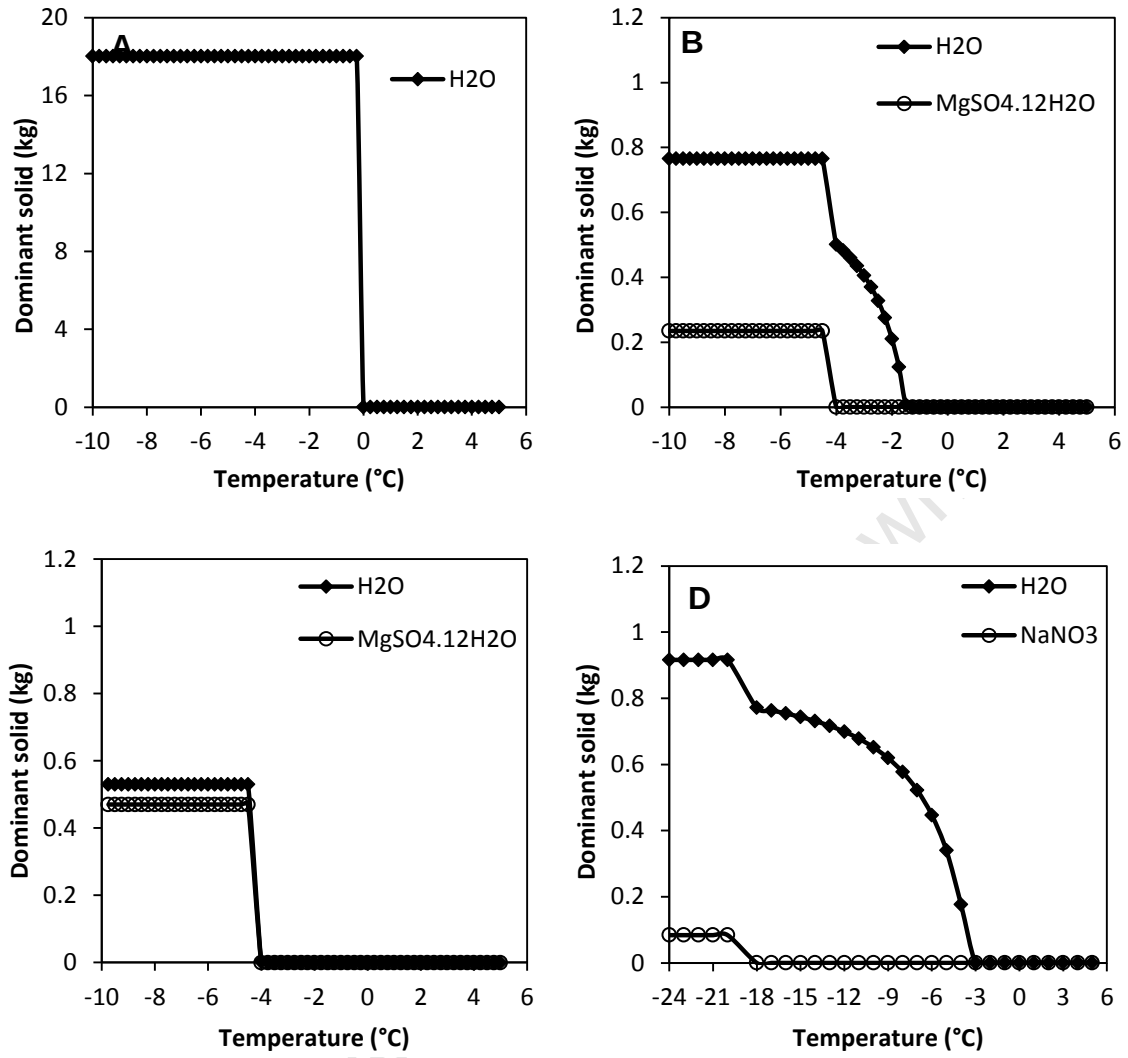

Figure 25: OLI Analyser predictions of ice nucleation temperatures for different systems; A – water; B – 8.4 wt% magnesium sulphate; C – 16.8 wt% magnesium sulphate; D – 8.4 wt% sodium nitrate

The results in Figure 25 did not take into account the metastability of the systems. However, they do show the effect of the solutes on the thermodynamic freezing point for ice. It can be seen that ice would crystallize at 0 °C pure water whereas the concentration of 8.4 wt% of magnesium sulphate depresses the freezing point to -1.5 °C and 16.8 wt% depresses the freezing point of ice to -4 °C. An 8.4 wt% of sodium nitrate depresses the freezing point to about -3 °C. This meant that the ice would not form until these temperatures are reached.

When the ice forms and begins to grow from a solution as in the case of Figure 25 B–D, the H_2O concentration reduces in the solution thus increasing the concentration of the solutes. The growth of ice is characterised by the rejection of the solutes that accumulate at the solid–liquid interface thereby creating a concentration gradient. The concentration gradient modifies the equilibrium temperatures by decreasing the equilibrium temperatures where the concentration is high. The decrease in equilibrium temperature results in a higher supercooling thus increasing the amount of supersaturation. Consequently, this may result in constitutional supercooling. Therefore, concentrations are expected to affect the thermodynamics of ice growth processes.

4.2 Analysis of ice growing in pure water

Figure 26 shows the refractive index-temperature relation of pure water generated using Equation 2-17 formulated by Harvey and co-workers (1998). It can be seen that the refractive index of water increases with the decrease in temperature up to 0 °C where it is highest with a value of 0.33435. Beyond that the refractive index begins to decrease (Harvey et al., 1998).

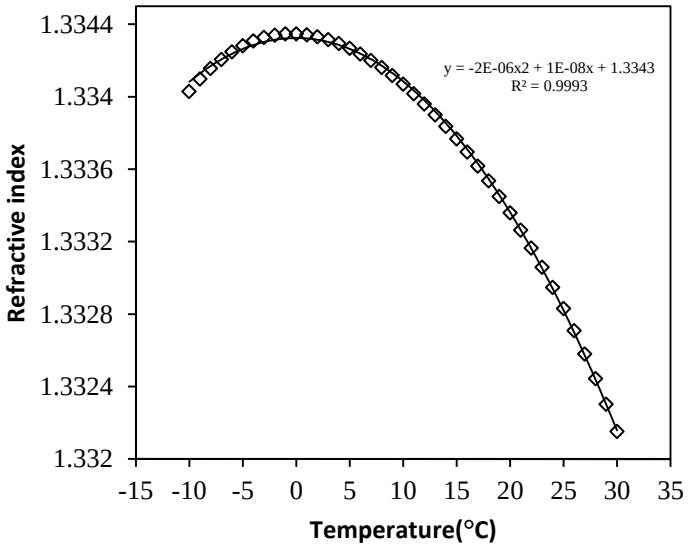

Figure 26: Refractive index of pure water as a function of temperature

The following figures present Schlieren images and graphs of refractive index of water before and during ice crystal growth. In image A of Figure 27, Figure 28 and Figure 29, it can be appreciated that the images were captured in-situ and that they were unprocessed. The corresponding images B–D were post processed in order to extract quantitative data using computational codes (see Appendix F) that were developed in Matlab®. Image processing involved the conversion of RGB values of the images to hue values in order to evaluate the gradient of refractive index. The images B's show the map of differential index of refraction. The images C show the differential index of refraction along the highlighted area in images B and the images D show the relative refractive index.

The highlighted areas along the vertical axis in the images B show the region where the refractive index was measured during crystallization process. Ice growth during layer growth was unidirectional.

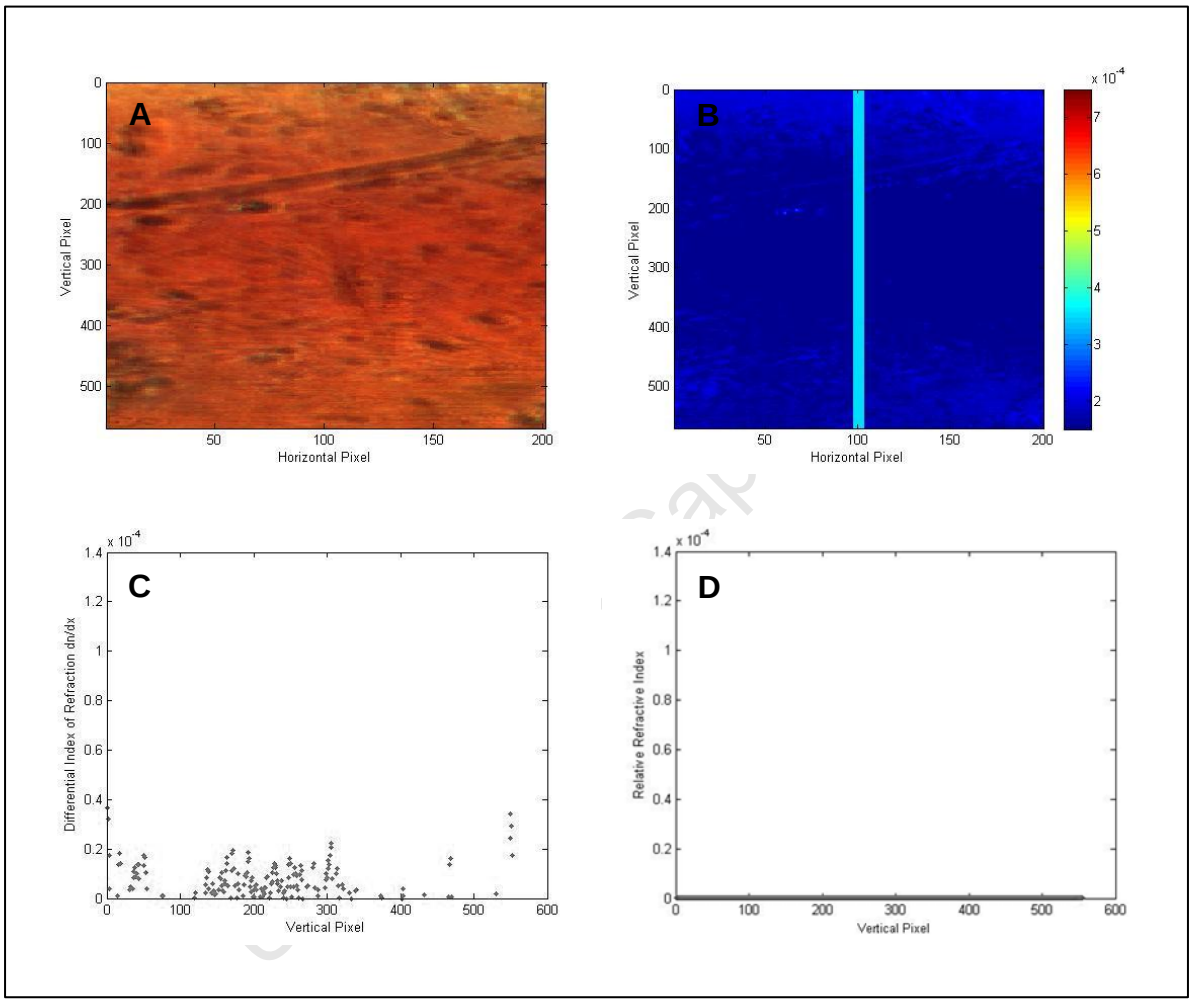

Figure 27: Initial image of de-ionised water before cooling: A – Unprocessed image; B – Map of differential index of refraction; C – Graph of differential index of refraction along the highlighted area in image B; D – Graph of relative refractive index along the highlighted area in image B.

Colour variations were observed when there were differences in the refractive index within the de-ionised water under investigation. The differences in refractive index were caused by the temperature gradients created when the water was cooled. During crystallization, the heat of crystallization also contributed to the change in temperature profiles of the cooled water.

It can be seen that at the beginning of the experiment in Figure 27, there was no temperature gradient. The distribution of colour in image A was uniform and the value of the differential index of refraction in images B and C was zero. Subsequently, the value of the relative refractive index in image D was also zero. This meant that at this stage, the water was homogeneous. Since temperature is the only parameter that affects the value of the refractive index in pure water, the spatial distribution of temperature was the same.

The introduction of heat transfer processes during cooling and crystallization resulted in the creation of temperature gradients as reflected in the gradients of refractive index of the water in Figure 28 and Figure 29. The temperature gradients were along the vertical direction. The colder regions were near the heat exchanger at the bottom of the test cell in the crystallizing chamber located at vertical pixel 590.The hotter regions were on locations away from the heat exchanger and the ice growing front towards the vertical pixel 0 in the images.

Figure 28 show the changes that occurred in the refractive index when cooling was introduced just before ice nucleated. It can be seen in image A of Figure 28 that the colour distribution varied vertically. The plot of a curve of the differential of refractive index corresponding to image A showed a depression between vertical pixels of 190 and 550. The subsequent plot of relative refractive index showed a peak at vertical pixel 490.

Based on the refractive index-temperature relation shown in Figure 26, this location was considered to be 0 °C and beyond this point between pixels 490 and 590 the water was supercooled. The peak was considered to be 0 °C because the temperature profile of the de-ionised water in the cell was known i.e. it decreased

vertically from vertical pixel 0 towards the vertical pixel 590 where the heat exchanger was situated.

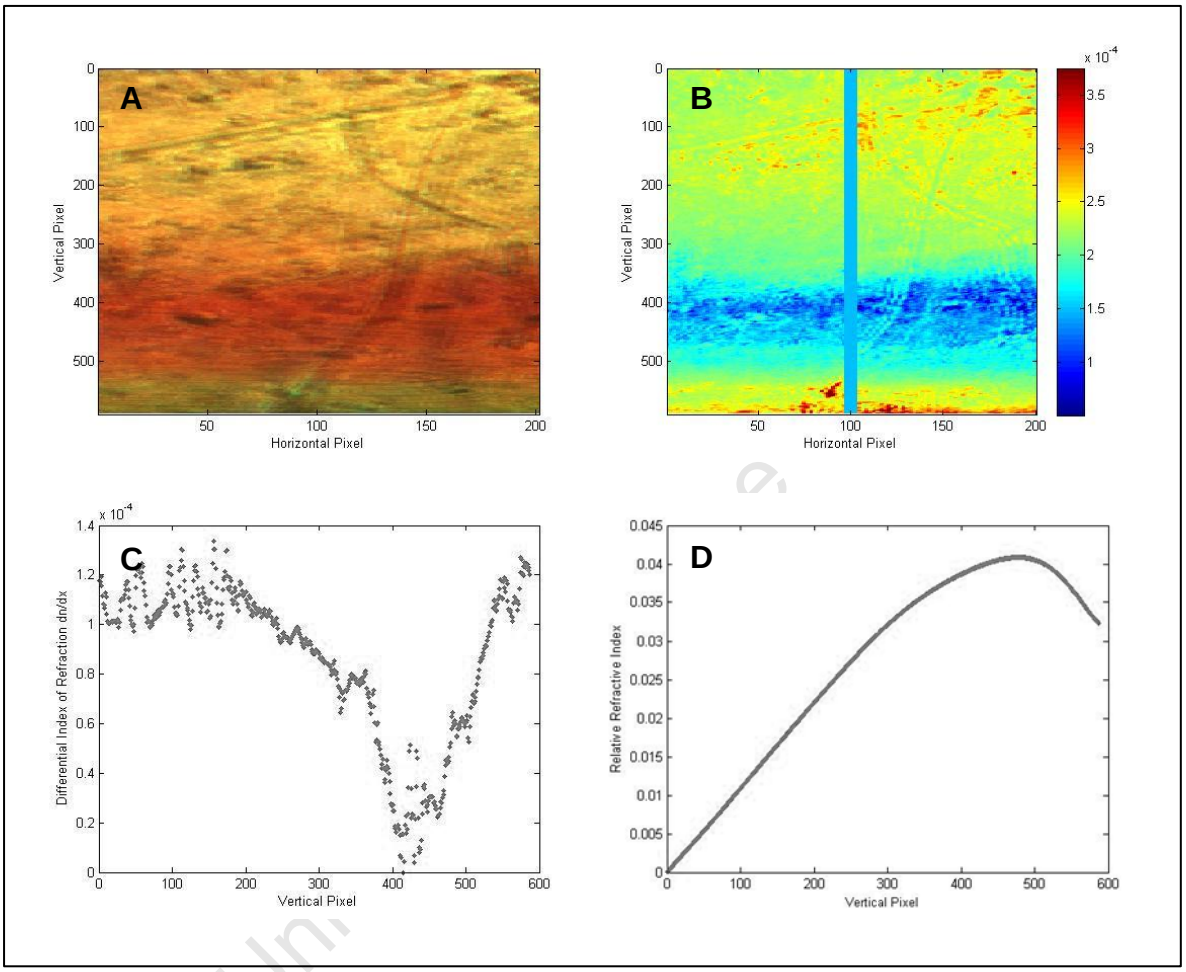

Figure 28: Image of de-ionised water just before nucleation of ice: A – Unprocessed image; B – Map of differential index of refraction; C – Graph of differential index of refraction along the highlighted area in image B; D – Graph of relative refractive index along the highlighted area in image B.

Figure 29 shows the changes that occurred in the refractive index of the de-ionised water during crystal growth. A colour distribution varying vertically was observed in image A. However, the variations were not as distinct as in image A of Figure 28. The corresponding values and the shapes of the differential of refractive index and the relative refractive index were also different. This was because of the change in the temperature profiles of the water before and during ice crystal growth.

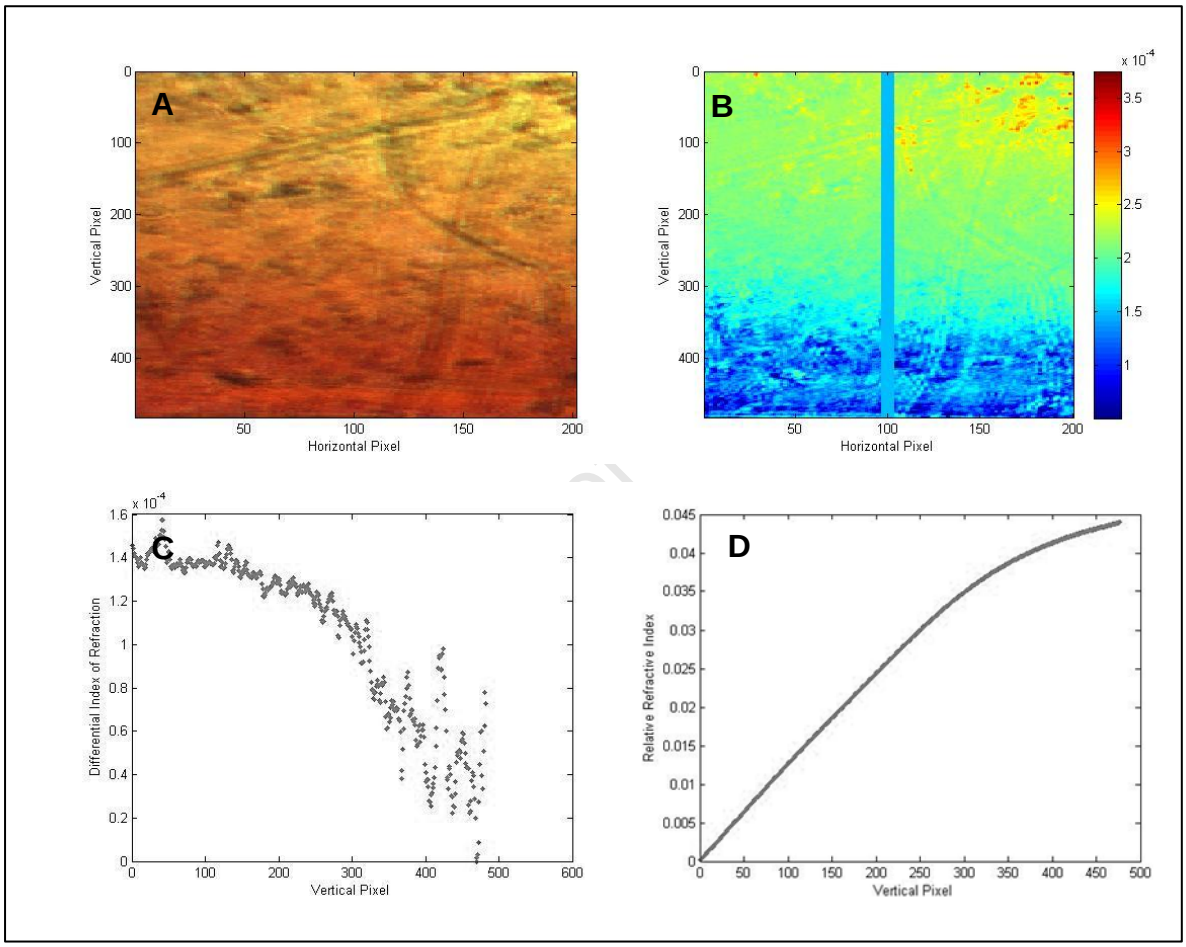

Figure 29: Image of de-ionised water during ice growth: A – Unprocessed image; B – Map of differential index of refraction; C – Graph of differential index of refraction along the highlighted area in image B; D – Graph of relative refractive index along the highlighted area in image B

The image C of Figure 29 showed a decrease in the differential index of refraction from vertical pixel 0 to vertical pixel 590. The subsequent corresponding relative reactive index showed an increase between these pixels. Compared to the gradient of the relative refractive index in image D of Figure 28 near the heat exchanger, the gradient of refractive index in Figure 29 near the surface of the growing ice was less steep. The reduction in the gradient of the refractive index was because of the release of heat of crystallization and the increased thermal resistivity by the crystalline layer which reduced the level of supercooling of the de-ionised water and the cooling rate respectively.

4.2.1 Temperature analysis

In order to obtain temperature measurements for a pure water sytem from the Schlieren images, the graphs of refractive index in images D of Figure 27, Figure 28 and Figure 29 were related to the refrative index –temperature curve in Figure 26 .The following section presents temperature results from the Schlieren technique.

Using Equation 2-17, the measured refractive index of the water during crystallization process from the Schlieren images was used for the spatial mapping of temperature. For example, the relative refractive index along the highlighted area shown in Figure 28 B was corrected to the absolute values within the boundary conditions. The absolute refractive index was then related to the above refractive index-temperature curve in Figure 26 to obtain the spatial map of temperature shown in Figure 30.

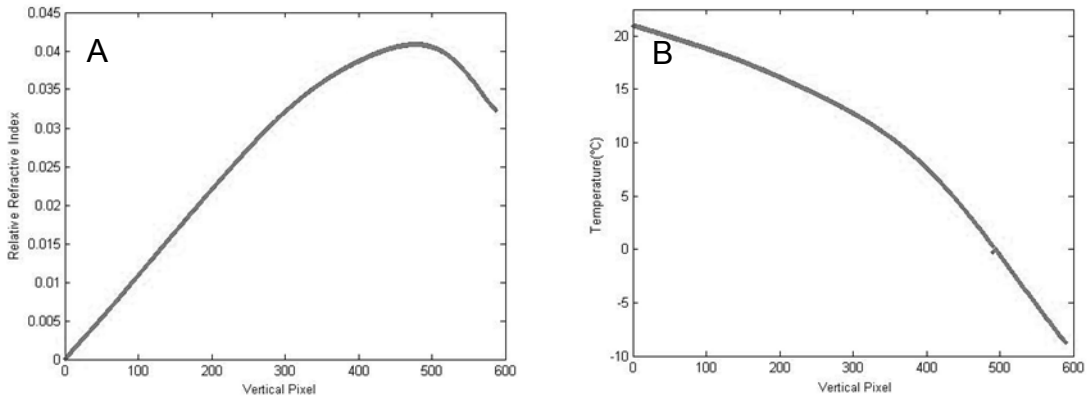

Figure 30: Refractive index and temperature; A – Refractive index of water just before nucleation; B – Corresponding temperature of the water

Figure 31 presents the evolution of the temperature profile of the de-ionised water before and during ice growth.

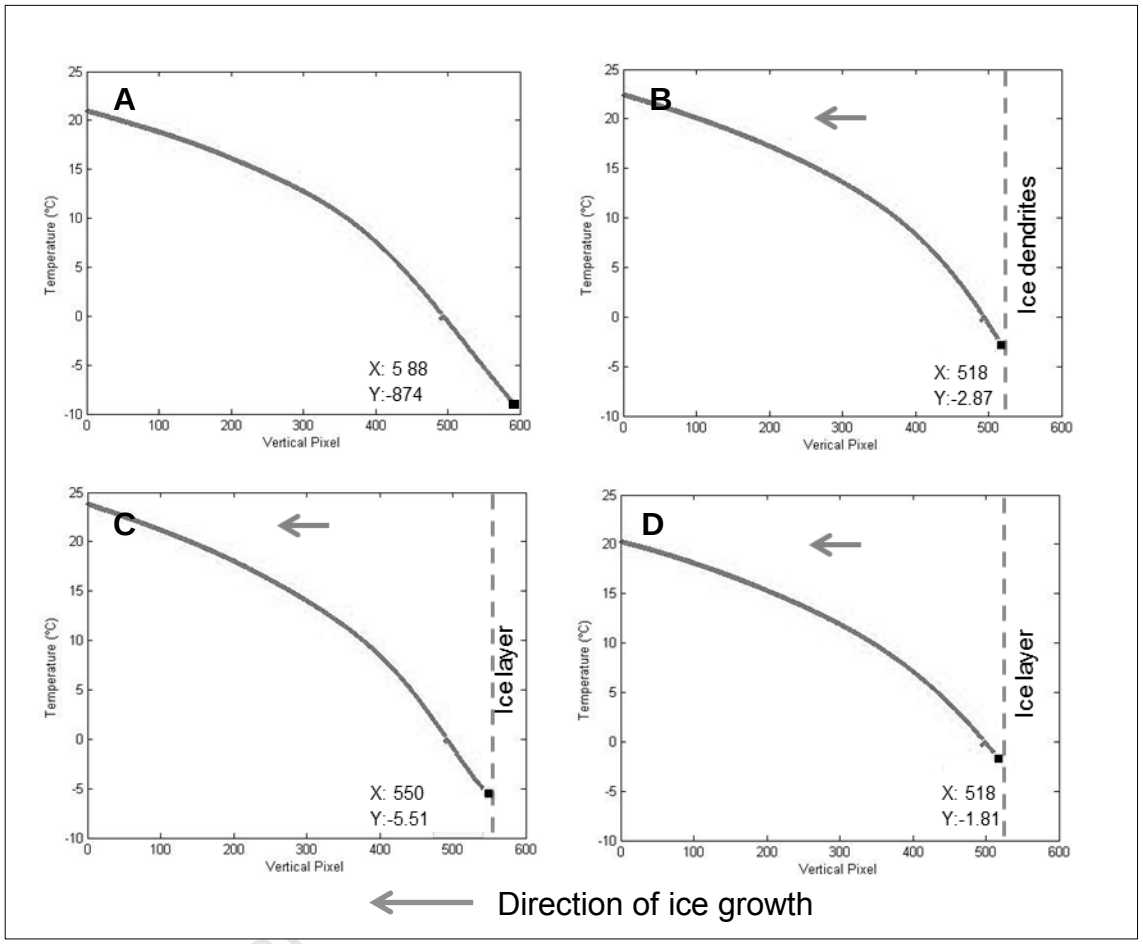

Figure 31: Temperature profile of de-ionised water before and during ice growth; A – Just before ice nucleation; B – During dendritic growth; C – Transition stage between dendritic and layered growth; D – 10 sec. after ice nucleation (layered growth)

It can be seen that the temperature profile changed with time. The temperature gradient was greatest at the time just before the ice nucleated. However, it drastically decreased during dendritic growth because of the release of heat of crystallization which caused the temperature of the de-ionised to increase as shown in Figure 31 A and B respectively.

At the transition stage when the type of growth changed from dendritic to layered, the temperature gradient again increased as can be seen in Figure 31 C. The increase of the temperature gradient was because of a higher supercooling. During layered growth, the temperature gradient decreased with time as shown in image Figure 31 D.

4.2.1.1 Effect of local supersaturation on growth rate and surface morphology

The spatial mapping of temperature enabled the measurements of temperature values of supercooled water up to locations of less than 10 μm away from the solid–liquid interface of ice during growth. Supercooling can be expressed as $\Delta T = T^* - T$, where T^* is the equilibrium melting temperature of ice i.e. 0 °C and T is temperature of the water below 0 °C. The temperature T was measured at locations of less 10 μm and was used to measure the supersaturation on the liquid side.

Figure 32 shows the temperature of supercooled water close to the solid–liquid interface of ice versus the growth and dissolution rate of ice.

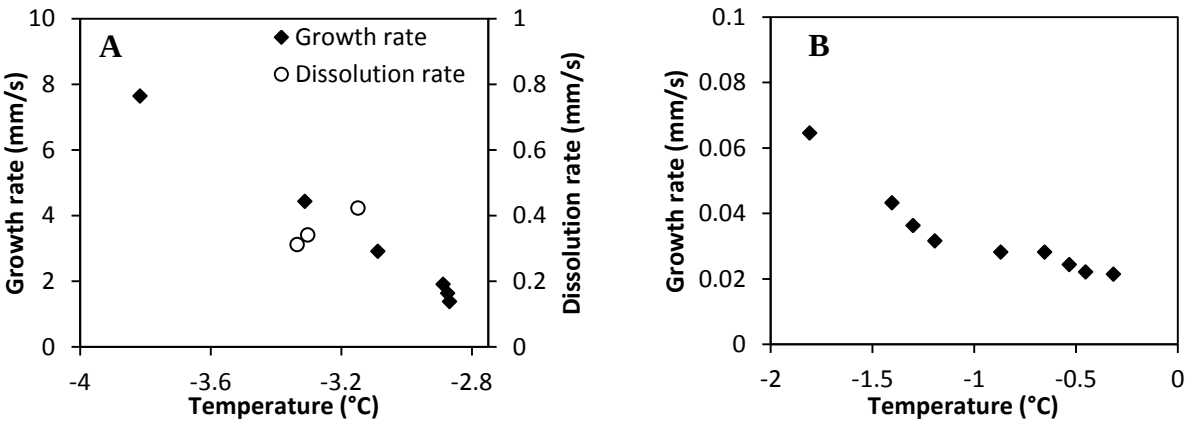

Figure 32: Growth and dissolution rate as a function of temperature of supercooled water near the ice-water interface: A – Dendritic growth; B – Layered growth

The removal of heat by cooling was responsible for the change in temperature profiles of the systems. However, during crystallization the temperature near the surface of the ice was affected by both the removal of heat by cooling and the diffusion of heat of crystallization into the liquid. It can be seen in Figure 32 that the growth rate decreased with an increase in T while the dissolution rate obtained during the melting of the dendrites increased with an increase in T.

Figure 33 shows the effect of local supersaturation on the growth rate of ice. The value of T (very close to the solid–liquid interface), determined the value of the local supersaturation which determines for crystal growth rate.

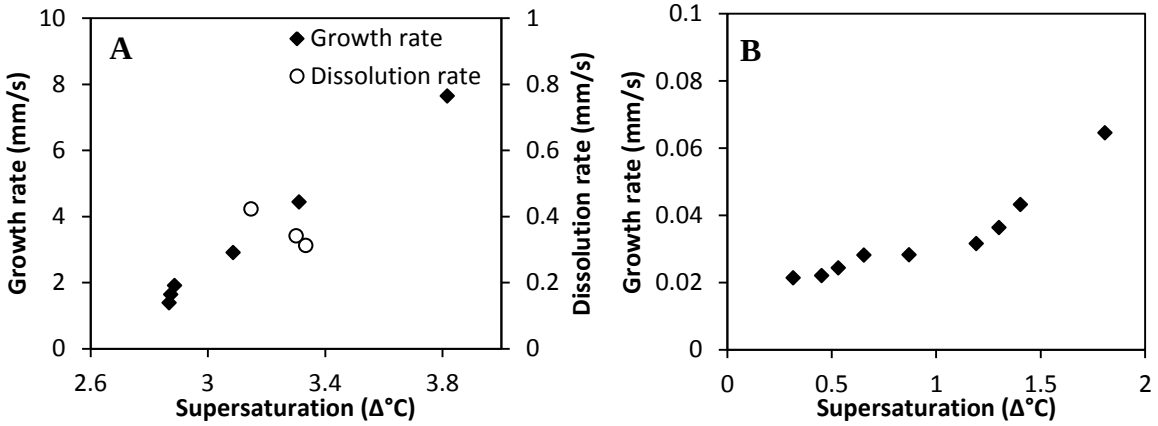

Figure 33: Effect of local supersaturation on growth rate; A – Dendritic growth; B – Layered growth

It can be seen in Figure 33 that higher local supersaturation resulted in a higher growth rate. A comparison of Figure 33 A and B showed that when the supersaturation was higher than 2.8, the growth rate was 100 times higher and the ice formed dendrites. Dendritic ice was observed at early stages of ice formation before it melted.

During dissolution of the dendrites, the rate of dissolution decreased with an increase in supersaturation. The other factor that affected the rate of dissolution was the amount of heat of crystallization which was absorbed by the dendrites. At supersaturations lower than 2.8, the ice surface was smooth at macroscopic scale and grew in layers.

Figure 34 and Table 4-1 show the two different morphologies of ice observed during crystallization at different supersaturations of the water.

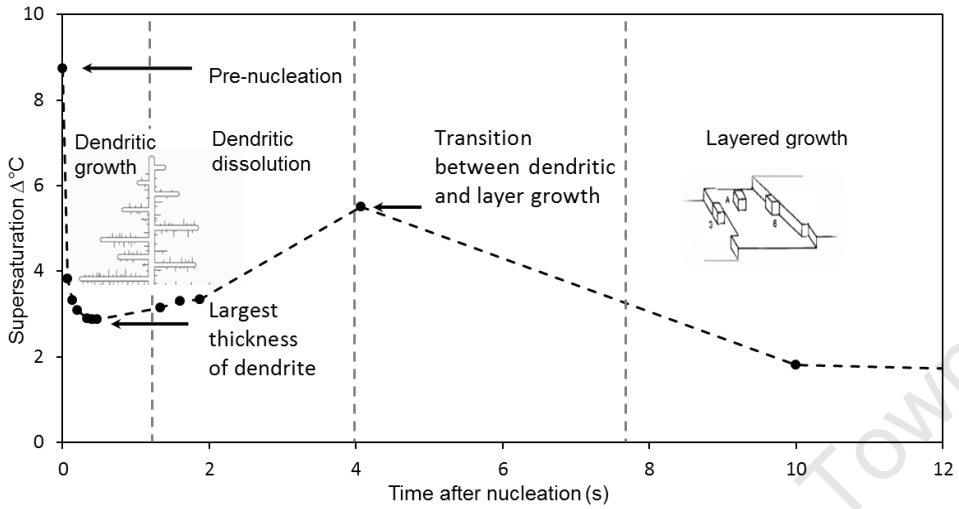

Figure 34: Type of growth during crystallization in de-ionised water

Table 4-1: Supersaturation levels at different stages of ice crystallization

Stage of process	Supersaturation	Type of growth
Just before nucleation	8.74	
Largest thickness of dendrite	2.87	Dendritic
Transition of dendritic to layer growth	5.51	
10 sec after nucleation	1.81	Layered

Dendrites form due to high supersaturation and low temperature gradients. The growth of ice dendrites in pure water is a diffusion–limited process where the transport of heat dictates the behaviour of the solid–liquid interface. Dendrites grow into regions of high supersaturation. The subsequent high release of the heat of crystallization results in the depletion of supersaturation in certain locations in the growing front thus, prevents the dendrites to grow further. It can be seen in Figure 34 that the temperature T which is related to supersaturation affected the growth of the dendrites. The heat that diffused into the water and the heat that was conducted by the dendrites controlled the growth rate, the extent of growth as well as the dissolution rate. Quantification of the amount of heat of crystallization that diffused into the liquid side during dendritic growth is presented in section 4.2.1.2.

It was observed that supersaturation increased during the transition stage of dendritic to layered growth. This stage was after the dendrites had melted but before the initiation of layered growth. This showed that a larger supersaturation was needed to prevent a complete melting of the ice and initiate layered growth. However, during layered growth, supercooling, hence supersaturation, was comparatively low and gradually decreased with time as can be seen in Figure 34. The increase in temperature during layered growth was due to the growth of ice into regions of lower supercooling coupled with the lower heat extraction by the heat exchanger as a result of increased thermal resistivity by the ice layer.

Comparatively, the ice dendrites formed in an 8.4 wt% magnesium sulphate solution were smaller than those in pure water. This is because dendritic formation of ice in a salt solution is not only affected by the heat diffusion but also by the diffusion of solute mass. In order for the ice to grow, water molecules in the solution have to be incorporated onto the ice crystal and at the same time, the solute mass must be transported away from the solid–liquid interface. The presence of the solutes hampers the transport and incorporation of the water molecules and could be the reason why the observed dendrites were smaller.

4.2.1.2 Quantification of heat transferred to the liquid side during dendritic growth

Figure 35 shows the graphs of heat flux as a function of growth rate during dendritic and layered growth.

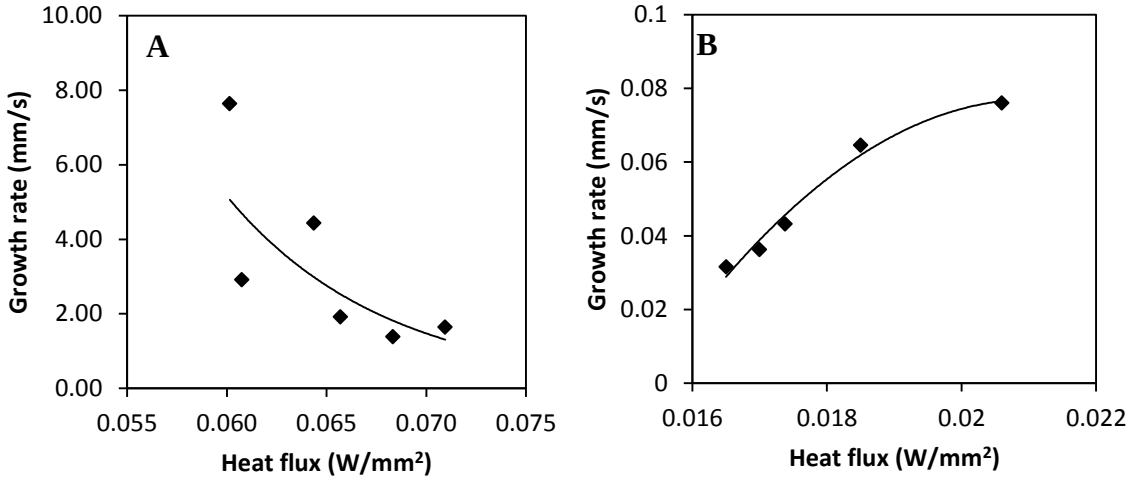

Figure 35: Effect of heat flux on growth rate; A – Dendritic growth; B – Layered growth

Heat flux is the rate of heat energy that is transferred through a surface. In this case, it was the rate of heat energy that was transferred from the liquid through the crystalline ice to the heat exchanger. It was therefore expected that an increase in heat fluxes should result in an increase in the growth rate. This was not true for ice dendritic growth, as can be seen in the trend in Figure 35 A. However, this was true with layered growth as shown in Figure 35 B.

In Figure 35 A, the growth rate of the dendrites decreased as the heat flux increased. This meant that the variations in crystal growth rate of the dendrites was not just dependant on the removal of heat from the system but also dependant on the diffusion of heat away from the growing fronts of the dendrites.

By using irreversible thermodynamics and the Onsager equations described in section 2.3.1 and Equation 2-15 and Equation 2-16 presented by Genceli and co-workers (2009), the ratio k was quantified. The ratio k is the heat transferred to the liquid side divided by the enthalpy of crystallization (Genceli et al., 2009).

Figure 36 presents the variation of the value of k during dendritic growth and its relationship with the growth rate. It can be seen from the figure that about 3%–16% of the heat of crystallization was transferred to the liquid side. The highest value of k (0.16) was when the dendrites reached maximum thickness before they started to melt.

As earlier discussed, both the 3%–16% transferred to the liquid side and the 84%–97% of the heat transferred to the ice side were responsible for controlling the growth dynamics of dendrites and the eventual partial dissolution of the ice during dendritic growth and dissolution.

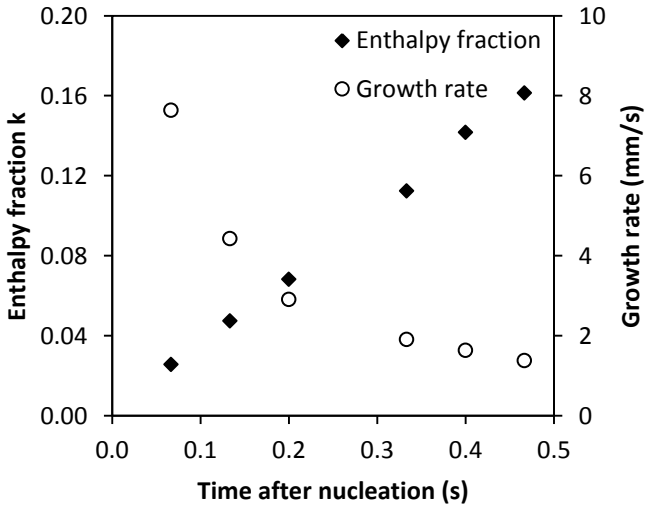

Figure 36: Enthalpy fraction k during dendritic ice growth

The results in Figure 36 demonstrate that heat of crystallization is not only transferred to the ice side but to the liquid side. It therefore agrees with current theories based on laws of irreversible thermodynamics coupled with Onsager equations.

The heat of crystallization during layered growth was however, not measured due to experimental limitation i.e. the detection of the amount of heat released during layered growth and the degree of temperature gradient in the growing front. However, it is expected that the value of k during layered growth would be less than the value of k during dendritic growth.

Compared to the k value of 20%–30% of magnesium sulphate of the heat transferred to the liquid side (Genceli et al., 2009), the k values for ice were less. One of the reasons for the difference could be in the difference in thermal conductivities between ice and water. The conductivity of ice at 0 °C is 0.0214 $Wcm^{-1}{}^{\circ}C^{-1}$ and for water at the same temperature of 0 °C it is 0.00561 $Wcm^{-1}{}^{\circ}C^{-1}$. This represents about a 3.8 times increase and hence it was expected that a much larger fraction of the heat would be conducted by the ice.

4.2.1.3 Comparison surface temperature of ice

The following presents a comparison of the data in literature and the one generated in this study. The major difference between the two sets of data in terms of generation is that the present data is obtained from in-situ measurements using non-intrusive technique which allows spatial mapping of the temperature gradient. This means that temperature readings can be obtained at any location within the field of view. More so, the ΔT in literature (referenced in this study) represents the difference between the equilibrium temperature and the amount of supercooling of the water. The supercooled water was considered uniform locally and temperature readings were obtained using traditional probes. However, in this work, because of capabilities to measure temperature within a temperature gradient field, the temperature difference (ΔT) between the equilibrium temperature and the liquid temperature near the solid–liquid interface measured.

Table 4-2 shows the variations in the value of ΔT for the Colour Schlieren data and the ones calculated from Equation 2-11 (Huige, 1972) and Equation 2-12 (Kallungal & Barduhn, 1977) and the growth rate obtained with the Colour Schlieren data.

The results show a difference of an average value of 0.58 °C lower than the results predicted by the Huige model and a value of 0.84 °C higher than the Kallungal model.

Table 4-2: Comparison of and supercooled temperature near the solid–liquid interface and predictions by the Huige and Barduhn growth rate correlations for layer growth

Growth rate *V* (mm/s)	**Supercooling ΔT (°C)**			**Difference with Schlieren**	
	Schlieren	**Huige**	**Kallungal**	**Huige**	**Kallungal**
0.065	1.81	0.50		1.31	
0.043	1.40	0.42		0.99	
0.036	1.30	0.39		0.91	
0.032	1.19	0.36		0.83	
0.028	0.87	0.34	1.49	0.52	0.62
0.024	0.53	0.32	1.39	0.21	0.86
0.022	0.45	0.31	1.33	0.14	0.88
0.021	0.31	0.30	1.31	0.01	1.00

4.3 Analysis of ice growing in a salt solution

4.3.1 Ice growth in magnesium sulphate

The following results are based on ice growth from a salt solution. They represent a semi-quantitative analysis of the data. This is because knowing the contribution of the concentration and the temperature on the gradient of the refractive index of a solution is necessary for quantifying temperature and concentration of the solution. It means that another technique that could measure either temperature or concentration needed to be incorporated so as to decouple the temperature and concentration. Alternatively, in cases where a model for mapping either temperature or concentration for specific conditions is available, it can be used to decouple the temperature and the concentration. An example is the diagnostic for temperature of burning fuel using a Colour Schlieren and a numerical model for determination of chemical composition of fuel (Feikema, 2004). The former could be presented due to limited time and the latter because of non-availability of models.

Figure 37 A shows a graph of the refractive index-temperature of 8.4 wt% magnesium sulphate generated from Equation 2-18 and Equation 2-19. Figure 37 B is a graph of refractive index–concentration for magnesium sulphate solution generated from data obtained from CRC Handbook of Chemistry and Physics (Lide, 2010).

It can be seen from the two graphs above that the refractive index increases with the decrease in temperature for magnesium sulphate solution of constant concentration and also increases with the increase in concentration at a constant temperature. This implies that, the coupled effect of temperature and concentration where temperature decreased and concentration increased during crystallization would definitely result in an increase in the refractive index of the solution.

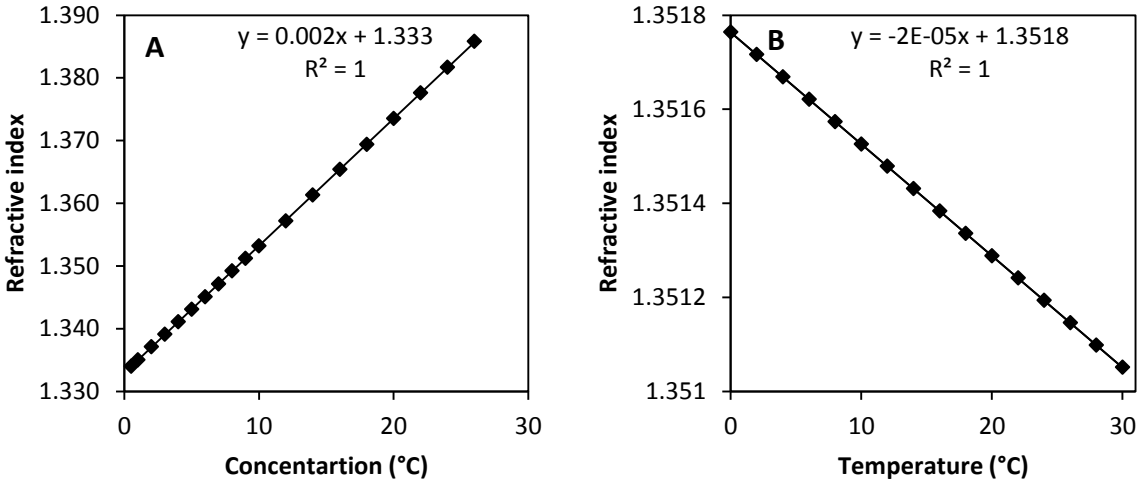

Figure 37: A – Refractive index as a function of concentration at 20 °C; B – Refractive index of 8.4 wt% of $MgSO_4$ as a function of temperature.

Figure 38 presents the Schlieren images of 8.4 wt% $MgSO_4$ solution before cooling. Unlike in the case for water in image A of Figure 27, the uniform colour in image A of Figure 38 implied uniformity in not only temperature but also in solute distribution of the solution. Therefore, there was no gradient in either temperature or concentration. However, during cooling and the subsequent crystallization, the temperature and concentrations gradients were created and evolved with time. Figure 39 and Figure 40 show images of 8.4 wt% $MgSO_4$ solution just before nucleation of ice and during ice growth.

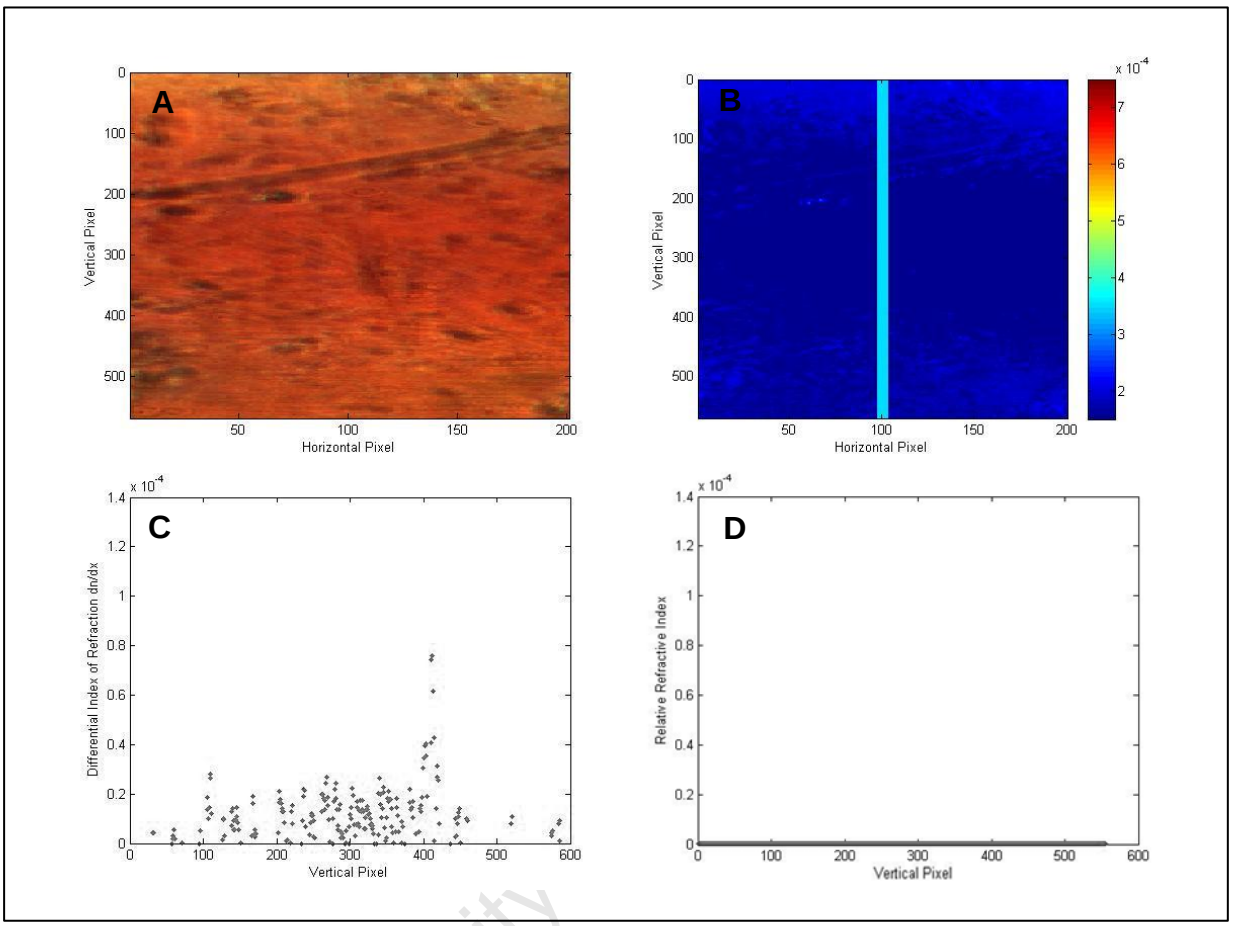

Figure 38: Initial image of 8.4 wt% MgSO4 solution before cooling: A – Unprocessed image; B – Map of differential index of refraction; C – Graph of differential index of refraction along the highlighted area in image B; D – Graph of relative refractive index along the highlighted area in image B.

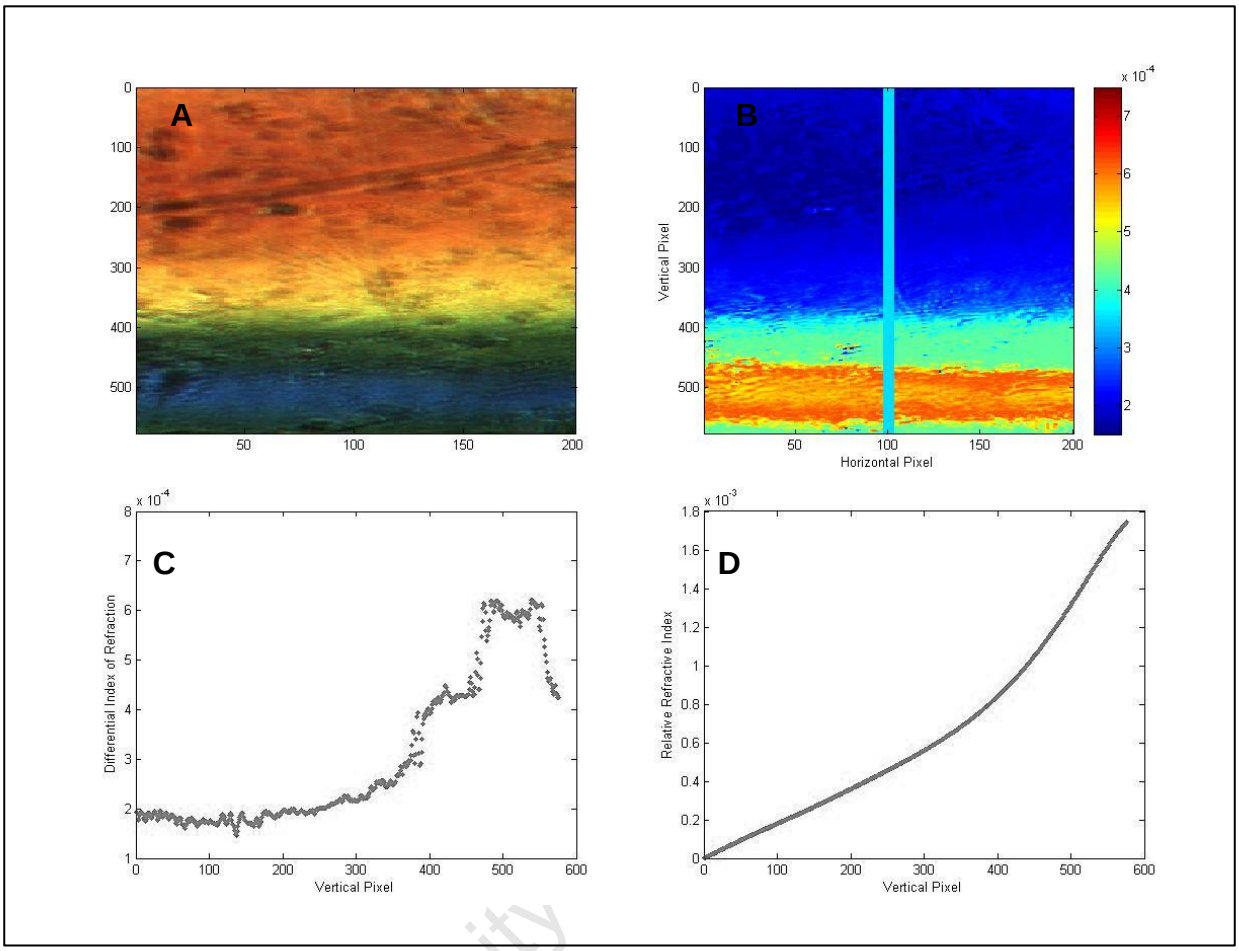

Figure 39: Image of 8.4 wt% $MgSO_4$ solution just before nucleation of ice: A – Unprocessed image; B – Map of differential index of refraction; C – Graph of differential index of refraction along the highlighted area in image B; D – Graph of relative refractive index along the highlighted area in image B.

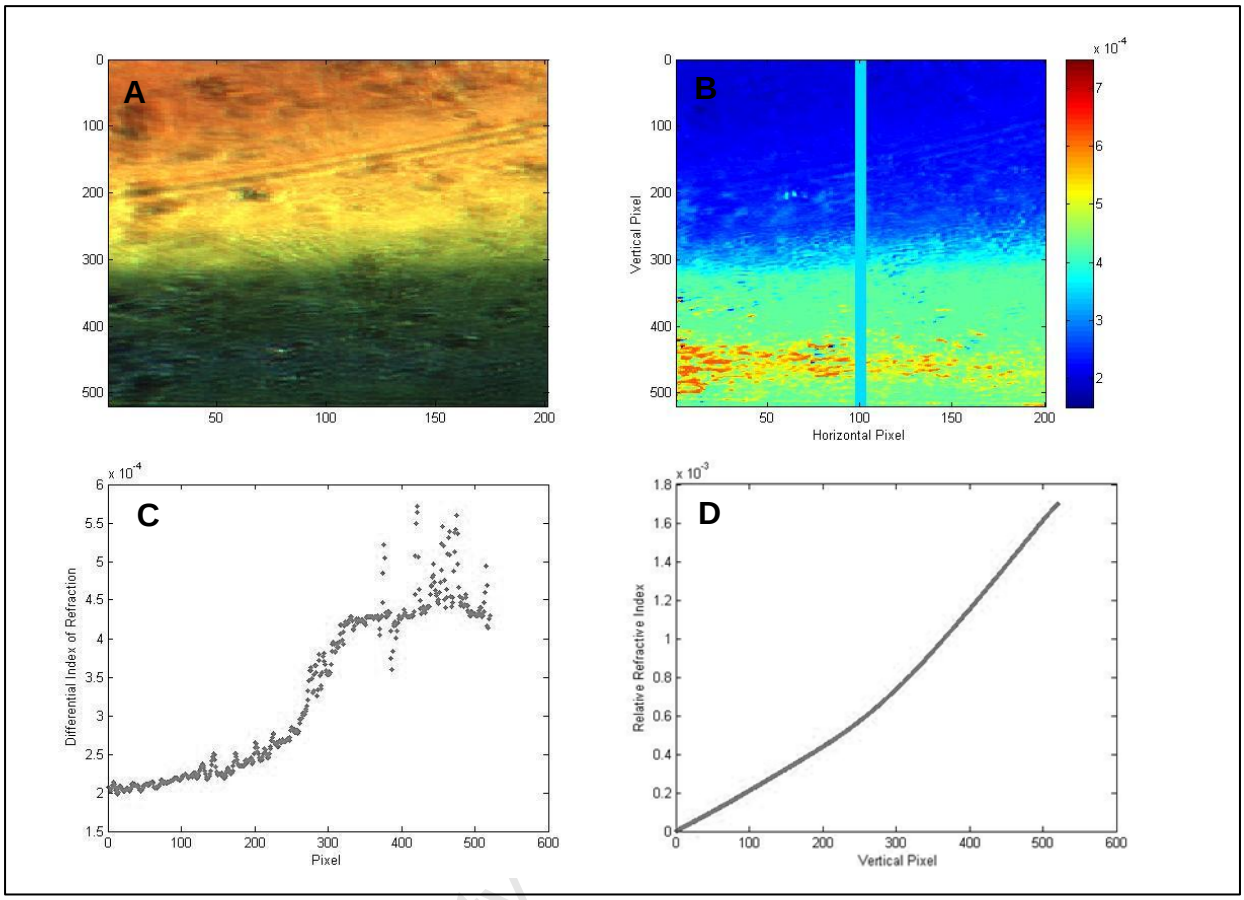

Figure 40: Image of 8.4 wt% $MgSO_4$ solution during ice growth: A – Unprocessed image; B – Map of differential index of refraction; C – Graph of differential index of refraction along the highlighted area in image B; D – Graph of relative refractive index along the highlighted area in image B.

Figure 41 presents the evolution the differential index of refraction of the solution before and during crystallization. Image A in Figure 41 shows the differential index of refraction just before nucleation while images B–D show the same graph at times 10, 20 and 30 seconds after nucleation respectively. Significant inhomogeneities were observed near the growing front of ice.

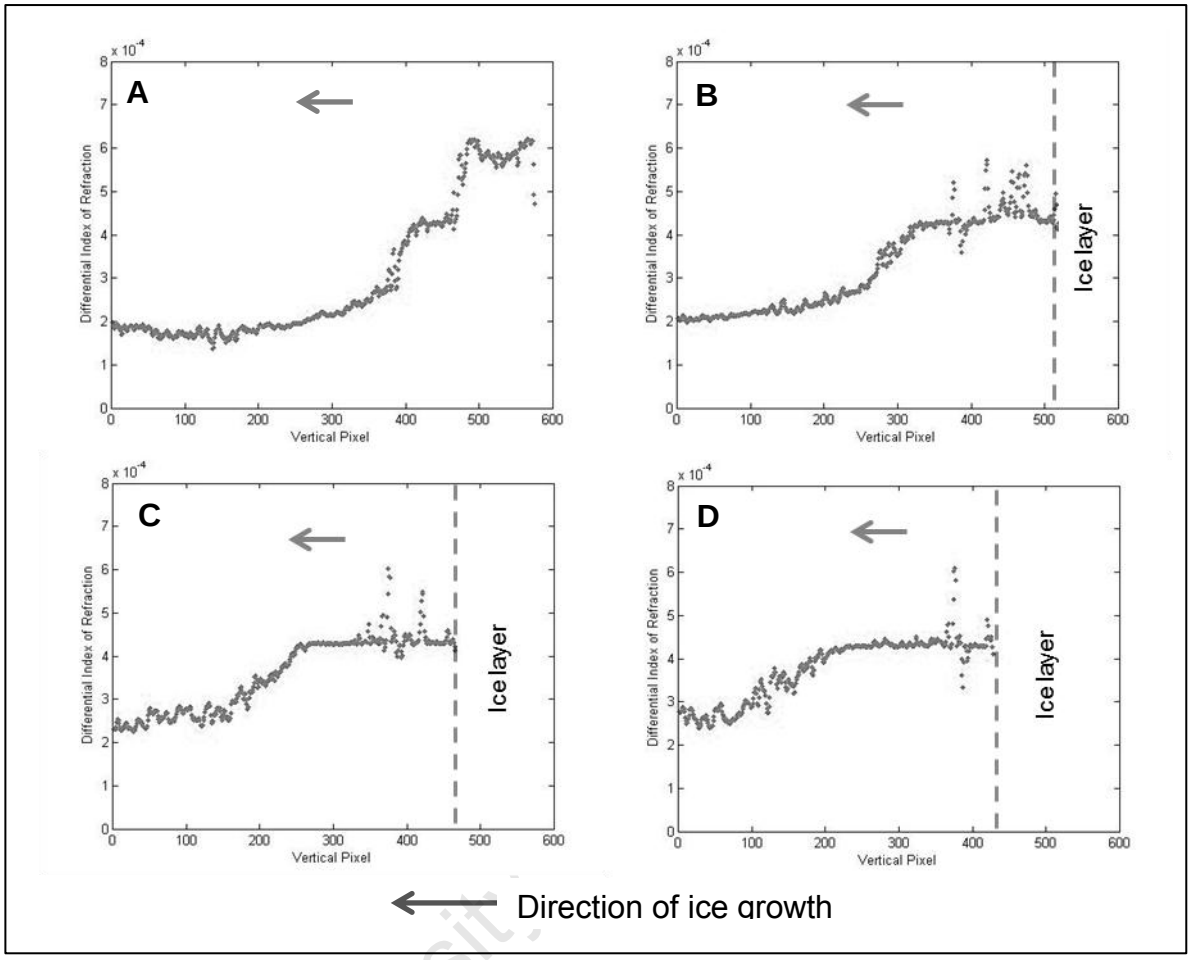

Figure 41: Evolution of refractive index gradient near the growing front of ice and the bulk solution; A – Just before nucleation of ice; B – 10 sec. after nucleation; C – 20 sec. after nucleation; D – 30 sec. after nucleation.

It can be seen that the gradient of refractive index decreased with time in the growing front of the ice. The highest gradient was observed just before ice nucleated and this can be attributed to the high temperature difference between the solution near the cooling surface (supercooled) and the solution in the bulk. However, during crystal growth, the gradient of the refractive index was affected by both the temperature and concentration gradients.

The temperature gradients were due to the removal of heat by cooling and the release of heat of crystallization. The concentration gradients were due to the decrease in the volume of the solvent (water) and the rejection and subsequent diffusion of the solutes from the growing ice.

Table 4-3 and Table 4-4 contain values obtained from curve fits in Figure 35 for magnesium sulphate solution with initial concentration 8.4 wt% during ice crystallization. Before the ice thickness reached 3mm, assuming that the ice that formed was 100% pure, it was calculated that the change in concentration in the solution would increase from 8.4 wt% to 14.9 wt%. The values for refractive index below 0 °C in Table 4-3 were obtained by extrapolating the fitted curve in Figure 37 B to -5 °C from 2 °C. The range was chosen because it was the range of temperature of the solution near the surface of the ice during ice.

The data presented in Figure 37 is more accurate for the temperature range of 0 °C and 40 °C. However, extrapolated values were made to postulate the change in magnitude of the refractive index assuming the refractive index increased linearly according to the curve fit.

Table 4-3: Change of refractive index with concentration

Conc. wt%	Refractive index
8.4	1.3498
9.4	1.3518
10.4	1.3538
11.4	1.3558
12.4	1.3578
13.4	1.3598
14.4	1.3698
14.9	1.3628

Table 4-4: Change of refractive index with temperature for 8.4 wt% $MgSO_4$

Temp. °C	Refractive index
-5	1.3519
-4	1.35188
-3	1.35186
-2	1.35184
-1	1.35182
0	1.35180
1	1.35178
2	1.35178

The two tables show that the values of the refractive index for different concentrations and temperatures vary in magnitude. The difference is in the order of one. However, what could not be established during the experiments were the gradients of temperature and concentration. In cases where the concentration gradients were lower than the temperature gradients, it was possible that the effect of temperature gradients on the gradient of refractive index was greater than that of the concentration.

The changes in the refractive index before crystallization and during dendritic growth were considered to be affected by temperature only. This is because of a uniform concentration distribution in the solution before crystallization and a comparatively faster diffusion rate of heat compared to mass solute.

4.3.2 Effect of solute concentration and solute specie on ice growth rate

Figure 42 presents the growth rate of ice in different systems as a function of time under the same subcooling. The growth rate reduced with time because of increased thermal resistivities as the crystalline ice grew.

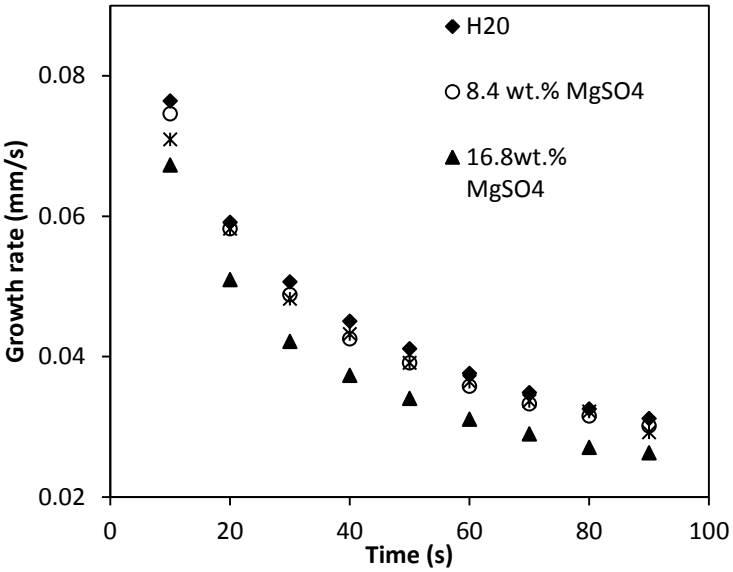

Figure 42: Ice growth rate as function of freezing time after nucleation.

It can be seen in Figure 42 that the growth rate of ice varied with the concentrations of the systems in which ice grew. Ice grew faster in pure water than solutions. The growth rate of ice in 8.4 wt% of magnesium sulphate and 8.4 wt% sodium nitrate was almost the same but much higher compared to ice grown in 16.8 wt%. It can be concluded that solutes concentration have an effect on the growth kinetics of ice.

The retardation in the growth rate was due to the influence of solutes on mass transport of the water molecules on the crystalline surface. Also, the concentrations at the solid–liquid interface changed the phase equilibrium temperatures and depressed the freezing point of the ice. Because the supercooling was the same, the ice grew fastest in a system (water) with a no freezing point depression followed by a system with a lesser freezing–point depression.

5 Conclusions and Recommendations

5.1 Conclusions

The concentration and temperature gradients between ice crystals and the surrounding solution are affected by heat and mass transfer processes which affects the nature of crystal growth. During crystallization, concentration and temperature gradients are caused by the generation of heat of crystallization and the increase of solute concentration in front of the growing ice crystal.

It was observed that some of the heat of crystallization was transferred to the liquid side and the some to the solid side. During dendritic growth, about 3%–16% of the heat of crystallization diffused in to the liquid ice and was responsible for the temperature increase on the liquid side. This heat coupled with the heat the remainder of 84%–97% conducted by the ice was responsible for partial melting of the dendrites before the initiation of layered growth. At the transition stage between dendritic growth and layered growth, a higher supersaturation was observed.

In the case of a pure water system, it was found that the ice growth rate increased with a decrease in temperature on the liquid side near the interface. The high growth rate led to dendritic growth and occurred at early stages of crystal formation due to high supersaturation. Once the metastable zone was broken, the supersaturation decreased and the lower growth rate resulted in layered growth.

When comparing ice surface temperature using two crystal growth models, a difference of 0.58 °C lower was observed when compared to the values predicted by the Huige model and 0.84 °C higher than the Kallungal model were found.

The ice growth rate in pure water was observed to be higher than in salt solution due to the mass diffusion of the solutes retarded the growth rate of ice in solutions. The retardation of the ice growth rate was due to the changes in the thermodynamic properties of the systems.

5.2 Recommendations

- Non-intrusive techniques offer better opportunities for more accurate quantitative temperature and concentration measurements compared to traditional probes. It has been demonstrated in this work that Colour Schlieren has a potential to obtain such measures. However, the major limitation is that it measures the refractive index influenced by both the temperature and concentration gradients. Therefore, there is a need to add another non-intrusive technique such as thermal chromatic liquid crystals which are sensitive to temperature only to decouple the two. This would enable quantification of empirical data generated.

- There is limited available data in literature of the change in refractive index with temperature for supercooled solutions. Therefore, there is a need to do experiments to generate data on refractive index for supercooled solutions since non-intrusive techniques depend so much on such parameters.

- The solid–liquid interface remains an area of interest for quantitative analysis since it is a region where most reactions and processes take place. Information that relates to mass and heat transports occurring during crystal growth at the interface can be measured more accurately by in situ measurements at a nanometer scale. This can be achieved by employing the methodology employed in this work by making improvements to the setup such as better filter design and the use of lenses with longer focal lengths, offers a great potential to achieve this.

- The study of ice growth mechanism in pure transparent solutions using Colour Schlieren has a lot of potential. For example, it can be used to study the structure of the ice during growth and ice melting in a salt solution. Melting of ice processes in water and salt solution is of particular interest in cold storage transport (Quarini & Chang, 2002) and in regions where snow forms where studies are carried out on how to best melt off the snow e.g. from the roads. Figure 43 A shows the Schlieren images of ice with potential further analysis for the study of the defection of in ice structure and Figure 43 B shows the Schlieren image of ice melting in a 16.8 wt% $MgSO_4$ with a potential for analysis for heat and mass transfer process during melting of ice in aqueous solution.

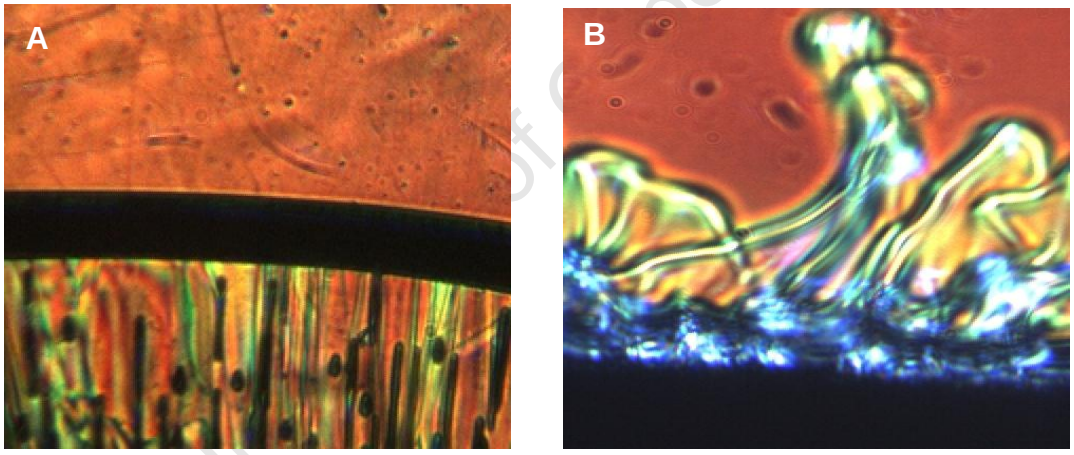

Figure 43: Schlieren image of ice; A – Channels and bubbles in ice growing from pure water; B – Ice melting in a 16.8 wt% magnesium sulphate solution

6 References

Akyurt, M., Zaki, G. & Habeebullah, B., 2002. Freezing phenonmena in ice -water system. *Energy Conversion and Management*, 43(14), pp.1773-89.

Ambrosini, D., Paoletti, D. & Rashidnia, N., 2008. Overview of diffusion measurements by optical techniques. *Optics and lasers in engineering*, 46(12), p.852– 864.

Angnes, L., Baptista, M.S. & Tumolo, T., 2004. Determination of the refractive index increment (dn/dc) of molecule and macromolecule solutions by surface plasmon resonance. *Analytical Biochemistry*, 333(2), pp.273-79.

Ayel, V. et al., 2006. Crystallisation of undercooled aqueous solutions: Experimental study. *International Journal of Heat and Mass Transfer*, 49(11-12), pp.1876-84.

Barduhn, A.J. & Huang, J.S., 1987. Why does ice grow faster from a salt water than from fresh water? *Desalination*, 67(3), pp.99-106.

Bennett, R.C., 2000. *Crystallization and Evaperation*. Boca Raton: CRC Press LLC.

Chen, X.D., Chen, P. & Free, K.W., 1997. A note on the two models of ice growth velocity in aqueos solutions derived from an irreversible thermodynamics analysis and the conversional heat and mass tranfer. *Journal of Food Engineering*, 31(3), pp.395-402.

Chen, P., Chen, X.D. & Free, K.W., 1998. Solute inclusion in ice formed from sucrose solutions on a sub-cooled surface-an experimental study. *Journal of Food Engineering*, 38(1), pp.1-13.

Chen, J. et al., 2008. Refractive index of aqueous solution of CdTe quantum dots. *Optics Communications*, 281(13), pp.3578-80.

Dhanaraj, G., Byrappa, K., Prasad, V. & Dudley, M., eds., 2010. *Springer Handbook of Crystal Growth*. Berlin: Springer-Verlag.

Feikema, A.D., 2004. *Quantitative rainbow schlieren deflectometry as a temperature diagnostic for spherical flames*. Ohio: National Aeronautics and Space Administration NASA-Glenn Research Center.

Genceli, F.E., 2008. *Eutectic Freeze Crystallization*. Phd Thesis. Deft: Deft University of Technology.

Genceli, F.E., Rodriguez-Pascual, M., Kjelstrup, S. & Witkamp, G., 2009. Coupled heat and mass transfer during crystallization of MgSO4.7H2O on a cooled surface. *Crystal growth and design*, 9(3), pp.1318-26.

Glicksmann, M.E. & Lupulescu, A.O., 2004. Dendritic growth in pure materials. *Journal of Crystal Growth*, 264(4), pp.541-49.

Goldstein, R.J., ed., 1996. *Fluid Mechanics Measurements*. New York: Taylor and Francis.

Grange, W.B., Viskanta, R. & Stevenson, W.H., 1976. Diffusion of heat and solute during freezing of salt solution. *International Journal of Heat Mass Transfer*, 19(4), pp.373-84.

Greenberg, P.S., Klimek, R.B. & Buchele, D.R., 1995. Quantitative rainbow schlieren deflectometry. *Applied Physics*, 34(19), pp.3810-22.

Gupta, A.S., Panigrahi, P.K., Muralidhar, K. & Gupta, R., 2010. Color Schlieren deflectometry for characterization of crystal growth. *Journal of Crystal growth*, 312(6), pp.817-30.

Hargather, M.J. & Settles, G.S., 2012. A comparison of three quantitative schlieren techniques. *Optics and Lasers in Engineering*, 50(1), pp.8-17.

Harvey, A.H., Gallagher, J.S. & Levelt Sengers, J.M.H., 1998. Revised Formulation for the Refractive Index of Water and Steam as a Function of Wavelength, Temperature and Density. *J.Phs. Chem. Ref Data*, 27(4), pp.761-74.

Hilson, G., 2000. Pollution prevention and clean production in the mining industry: An analysis of currrent issues. *Journal of Cleaner Production*, 8(2), pp.119-26.

Holman, J.P., 1981. *Heat Transfer*. 5th ed. New Yolk: McGraw-Hill, Inc.

Huige, N.J.J., 1972. *Nucleation and growth of ice crystals from water and sugar solutions in continous stirred tank crystallizers*. PhD Thesis. Eindhoven: Eindhoven University of Technology.

Jackson, K., 2004. *Kinetic Processes: Crystal growth, Diffusion and Phase Transitions*. Weinheim: WEILEY-VCH Verlag and Co.

Jones, M.J. & Ulrich, J., 2006. *Heat and Mass Transfer Operations-Crystallization*. Oxford: Eolss.

Kallungal, J.P. & Barduhn, A.J., 1977. Growth rate of an ice crystal in subcooled pure water. *American Institute of Chemical Engineers*, 23(3), pp.294-303.

Kim, K.J. & Ulrich, J., 2001. Theoretical and experimental studies on the behaviour of liquid impurity in solid layer melt crystallization. *Journal of Physics D: Applied Physics*, 34(9), pp.1308-17.

Kjelstrup, S. & Bedeaux, D., 2008. *Non-Equilibrium Thermodynamics of Heterogeneous Systems*. Singapore: World Science Publishing Co.Pte.Ltd.

Lewis, A.E. et al., 2010. Design of a Eutectic Freeze Crystallization process for multicomponent waste water stream. *Chemical Engineering Research and Design*, 88(9), pp.1290-96.

Leyendekkers, J.V. & Hunter, R.J., 1977. Refractive index of aqueous electrolyte solutions: Extrapolations to other temperatures, pressures, wavelengths and multicomponet systems. *Journal of Chemical Engineering Data*, 22(4), pp.427-31.

Libbrecht, K.G., 2005. The physics of snow crystals. *Rep. Prog Physics*, 68(4), pp.855-95.

Lide, D.R., ed., 2010. *CRC Handbook of Chemistry and Phyisics*. 90th ed. Boca Raton, Florida: CRC Press/Taylor and Francis.

Lorain, O., Thiebaud, P., Bardorc, E. & Aurelle, Y., 2001. Potential of freezing in wastewater: soluble pollutant applications. *Water Research*, 35(2), pp.541-47.

Luo, C., Chen, W. & Han, W., 2010. Experimental study on factors affecting the quality of ice crystal during the freezing concentration for the brackish water. *Desalination*, 260(1-3), p.231–238.

Meewisse, J.W. & Ferreire, I.C.A., 2003. Validation of the use of heat transfer models in liquid/solid fluidized beds for ice slurry generation. *International Journal of Heat and Mass Transfer*, 46(19), pp.3683-95.

Mersmann, A., 2001. *Crystallization Technology Handbook*. 2nd ed. New York: Marcel Dekker Inc.

Mullin, J.W., 2001. *Crystallization*. 4th ed. London: Butterworth Heinemann.

Mullin, J.W., 2002. Crystallization and Precipitation. In *Ullmann's Encyclopaedia of Industrial Chemistry*. Online ed. New York: John Wiley and Sons, Inc. pp.1-51.

Myerson, A.S., 2000. *Industrial Crystallization and Precipitation*. PAON Course.

Myerson, A.S., 2002. *Handbook of Industrial Crystallization*. 2nd ed. Boston: Butterworth Heinemann.

OLI Systems Inc, OLI Stream Analyser, Verson 3.0, Morris Plains, New Jersey, USA, 2012.

Palaniappan, M. et al., 2010. *Clearing the waters- A focus on water quality solutions*. Oakland: UNON Publishing Services United Nations Environment Program.

Payne, A. & Mills, E., 2011. *Heat and mass transfer measurements during ice crystallization using digital imaging techniques*. UG Thesis. Cape town: University of Cape Town.

Petzold, G. & Aquilera, J.M., 2009. Ice morphology: Fundamental and technological application in foods. *Food Biophysics*, 4(4), pp.378-96.

Pronk, P., 2006. *Fluidized bed heat exchangers to prevent fouling in ice slurry systems and industrial crystallizers*. PhD Thesis. Delft: Delft University of Technology.

Pronk, P., Ferreira, C.A. & Witkamp, G.J., 2008. Prevention of crystallization fouling during eutectic freeze. *Chemical Engineering and Processing: Process Intensification*, 47(12), pp.2140-49.

Quarini, G.L. & Chang, Y.C., 2002. Heat transfer characteristics of ice melting in water and salt solutions. *Chemical Engineering Research and Design*, 80(3), pp.320-24.

Randall, D.G., 2010. *Development of a Brine Treatment Protocol using Eutectic Freeze Crystallization, PhD Thesis*. South Africa: University of Cape Town.

Ratkje, S.K. & Flesland, O., 1995. Modelling the freeze concentration process by irreversible thermodynamics. *Journal of Food Engineering*, 25(4), pp.553-67.

Rodriguez-Pascual, M., 2008. *Physical Aspects of Scraped Heat Exchanger Crystallizers-An Application in Eutectic Freeze Crystallization*. PhD Thesis. Deft: Delft University of Technology.

Sangwal, K., 2011. Recent developments in understanding of the metastable zone width. *Journal of Crystal Growth*, 318(1), pp.103-09.

Sato, K., Furukawa, Y. & Nakajima, K., eds., 2001. *Advances in Crystal Growth Research*. 1st ed. Amsterdam: Elsevier.

Schiebener, P., Straub, J., Levelt Sengers, J.M.H. & Gallagher, J.S., 1990. Formulation for the refractive Index of Water and Steam as a Function of Wavelength, Temperature and Density. *Phys.Chem.Ref.Data*, 19(3), p.677.

Sei, T., Gonda, T. & Arina, Y., 2002. Growth rate and morphology of ice crystals growing in a solution of trehalose and water. *Journal of Crystal Growth*, 240(1-2), pp.218-29.

Seithia, A., Semwal, K., Panigrahi, P.K. & Muralidhar, K., 2010. *Laser and Colour Schlieren measurement of a KDP crystal growth process*. Presentation. Kanpur: Indian Institute of Technology Kanpur.

Settles, G.S., 2001. *Schlieren and Shadowgraph Techniques*. New York: Springer-Verlag.

Shibkov, A.A. et al., 2003. Morphology diagram of nonequilibrium patterns of ice growing in supercooled water. *Physica A*, 319(1), pp.65-79.

Shlichta, S. & Verma, P.J., 2008. Imaging techniques for mapping solution parameters, growth rate, and surface features during the growth of crystal from Solution. *Progress in crystal growth and characterization of materials*, 54(1-2), pp.1-120.

Srivastava, A., Murallidha, K. & Panigrahi, P.K., 2004. Comparison of Interferometry, Schlieren and Shadowgraphy for visualizing covection around KDP. *Cystal Growth*, 261(1-2), pp.348-61.

Stasiek, J.A. & Kowalewsk, T.A., 2002. Thermochromatic liquid crystals applied for heat transfer research. *Opto-Electronics Review*, 1(10), pp.1-10.

Terwilliger, J.P. & Dizio, S.F., 1970. Salt rejection phenomena in the freezing of saline solutions. *Chemical Engineering Science*, 25(8), pp.1331-49.

Ulrich, J. & Stelzer, T., 2011. Kirk-Othmer Encyclopedia of Chemical Technology. In *Crystallization*. Online ed. New York: John Willey and Sons, Inc. pp.1-63.

van der Ham, F., Witkamp, G.J., de Graauw, J. & van Rosmalen, G.M., 1999. Eutectic Freeze Crystallization simultaneous formation and separation of two solid phases. *Journal of Crystal Growth*, 198-199, pp.744-48.

Van der Ham, F., Witkamp, G.J., De Graauw, J. & van Rosmalen, G.M., 1998. Eutectic Freeze Crystallization: Application to process streams and waste water purification. *Chemical Engineering Process*, 37(2), p.207–213.

Van't Land, C.M., 2005. *Industrial Crystallization of Melts*. New york: Marcel Dekker.

Venter, G.A., 2011. *http://www.scientificomputing.com*. [Online].

Wang, Z.L., Liu, Y. & Zhang, Z., eds., 2003. *Nanophase and Nanostructure Materials-Synthesis*. New York: Kluwer academic/Plenum Publishers.

Welty, J.R., Wicks, C.E., Wilson, R.E. & Rorrer, G.L., 2007. *Fundamentals of Momentum, Heat and Mass Transfer*. 5th ed. Hoboken: John Wiley and sons.

Yang, J.S., Hong, C.H. & Choi, G.M., 2007. Heat transfer measurements using thermochromatic liquid crystals. *Current Applied Physics*, 7(4), pp.413-20.

Appendices

Appendix A

Coefficients of formulation of refractive index of water

Nomenclature

n	refractive index
P_{sat}	saturation pressure
T	absolute pressure, IT-90
t	temperature in degrees Celsius
λ	wavelength of light
ρ	mass density

Reference constants

Reference temperature	T^*=273.15K
Reference density	ρ^*=1000 kg m^{-3}
Reference wavelength	λ^*=0.589$_{\mu m}$

Dimensionless variables

Temperature	$\bar{T} = T/T^*$
Density	$\bar{\rho} = \rho/\rho^*$
Wavelength	$\bar{\lambda} = \lambda/\lambda^*$

Table A 1: Coefficients of the formulation

$a_0 = 0.244\ 257\ 733$	$a_4 = 1.589\ 205\ 70x10^{-3}$
$a_1 = 9.746\ 344\ 76x10^{-3}$	$a_5 = 2.459\ 342\ 59x10^{-3}$
$a_2 = -3.732\ 349\ 96x10^{-3}$	$a_6 = 0.900\ 704\ 920x10^{-3}$
$a_3 = 2.686\ 784\ 72x10^{-4}$	$a_7 = -1.666\ 262\ 19x10^{-2}$
$\bar{\lambda}_{UV} = 0.229\ 202\ 0$	$\bar{\lambda}_{UV} = 5.432\ 937$

Appendix B

Table B 1: Thermal pproperties of water

Heat of fusion h_f	333.6 j/g
Density ρ at 0 °C	9.16×10^{-4} g/mm^3
Thermal conductivity k	5.16×10^{-3} W/ °C.mm

Appendix C

Table C 1: Measured and calculated data for Ice growing in pure water

Description	Frame	Time (sec)	Pixel at heat exchanger	Pixel at eq. temp	Lowest supercooling		Equilibrium temp.	Supercooling	Temp. gradient	Ice thickness	Ice growth rate
					Pixel	Temp. (°C)	(°C)	Δ °C	(°C/mm)	(mm)	(mm/sec)
Just before nucleation	1056	0.00	589	494	589	-8.74	0	8.74	10.12	0.00	0.0000
Dendritic growth	1057	0.07	589	494	533	-3.82	0	3.82	10.76	0.51	7.6385
	1058	0.13	589	490	524	-3.31	0	3.31	10.71	0.59	4.4331
	1063	0.47	589	494	518	-2.87	0	2.87	13.14	0.65	1.3835
	1076	1.33	589	490	527	-3.15	0	3.15	9.36	0.56	0.4228
	1080	1.60	589	493	529	-3.30	0	3.30	10.07	0.55	0.3410
	1084	1.87	589	490	525	-3.33	0	3.33	9.64	0.58	0.3118
Initial layer growth	1117	4.07	589	492	555	-5.51	0	5.51	9.62	0.35	0.0760
Layered growth	1206	10.00	589	495	518	-1.81	0	1.81	8.64	0.65	0.0646
	1356	20.00	589	475	494	-1.40	0	1.40	8.12	0.86	0.0432
	1507	30.07	589	451	469	-1.30	0	1.30	7.94	1.09	0.0363
	1656	40.00	589	433	450	-1.19	0	1.19	7.71	1.26	0.0316
	1806	50.00	589	421	434	-0.87	0	0.87	6.17	1.41	0.0282
	1957	60.07	589	399	403	-0.65	0	0.65	13.13	1.69	0.0282
	2106	70.00	589	399	402	-0.53	0	0.53	19.49	1.70	0.0243
	2256	80.00	589	379	395	-0.45	0	0.45	3.10	1.76	0.0221
	2407	90.07	589	373	377	-0.31	0	0.31	8.65	1.93	0.0214

Table C 2: Measured and calculated data for heat and mass fluxes during dendritic growth

Time after nucleation (s)	Temp. gradient (°C/mm)	Growth rate *v* (mm/s)	Heat flux $J_q^{',I}$ (W/mm^2)	Mass flux J ($g/mm^2.s$)	Heat transfer coeff. ratio $q^{*,I}$ (J/g)	Fraction of enthalpy k
0.0667	10.7219	7.6385	0.0602	0.0070	8.5901	0.0257
0.1333	11.4722	4.4331	0.0644	0.0041	15.8371	0.0475
0.2000	10.8301	2.9099	0.0608	0.0027	22.7765	0.0683
0.3333	11.7096	1.9096	0.0657	0.0018	37.5256	0.1125
0.4000	12.6464	1.6368	0.0709	0.0015	47.2822	0.1417
0.4667	12.1790	1.3835	0.0683	0.0013	53.8722	0.1615

Table C 3: Measured and calculated data for growth rate of ice in different systems during layered growth

Time after nucleation (s)	Growth rate (mm/s)			
	Water	8.4 wt.% $MgSO_4$	8.4 wt.% $MgSO_4$	8.4 wt% $NaNO_3$
10	0.0764	0.0746	0.0673	0.0709
20	0.0591	0.0582	0.0509	0.0582
30	0.0506	0.0488	0.0421	0.0482
40	0.0450	0.0425	0.0373	0.0432
50	0.0411	0.0391	0.0340	0.0391
60	0.0376	0.0358	0.0311	0.0364
70	0.0348	0.0333	0.0290	0.0336
80	0.0325	0.0315	0.0271	0.0322
90	0.0311	0.0301	0.0263	0.0292

Appendix D

Table D 1: Nucleation temperatures of ice of various systems (Modelled using OLI Stream Analyzer 2.0)

Pure water		8.4 wt% MgSO4			16.8 wt% MgSO4			8.4 wt% NaNO3		
Temp. (°C)	Solid H2O (Kg)	Temp. (°C)	Solid H2O (kg)	Solid MgSO4.12H2O (kg)	Temp. (°C)	Solid MgSO4.12H2O (kg)	Solid H2O (kg)	Temp. (°C)	Solid H2O (kg)	Solid NaNO3 (kg)
5.0	0	5.0	0	0	5.0	0	0	5	0	0
4.8	0	4.8	0	0	4.8	0	0	4	0	0
4.5	0	4.5	0	0	4.5	0	0	3	0	0
4.3	0	4.3	0	0	4.3	0	0	2	0	0
4.0	0	4.0	0	0	4.0	0	0	1	0	0
3.8	0	3.8	0	0	3.8	0	0	0	0	0
3.5	0	3.5	0	0	3.5	0	0	-1	0	0
3.3	0	3.3	0	0	3.3	0	0	-2	0	0
3.0	0	3.0	0	0	3.0	0	0	-3	0	0
2.8	0	2.8	0	0	2.8	0	0	-4	0.176	0
2.5	0	2.5	0	0	2.5	0	0	-5	0.340	0
2.3	0	2.3	0	0	2.3	0	0	-6	0.447	0
2.0	0	2.0	0	0	2.0	0	0	-7	0.522	0
1.8	0	1.8	0	0	1.8	0	0	-8	0.577	0
1.5	0	1.5	0	0	1.5	0	0	-9	0.619	0
1.3	0	1.3	0	0	1.3	0	0	-10	0.652	0
1.0	0	1.0	0	0	1.0	0	0	-11	0.678	0
0.8	0	0.8	0	0	0.8	0	0	-12	0.699	0
0.5	0	0.5	0	0	0.5	0	0	-13	0.717	0
0.3	0	0.3	0	0	0.3	0	0	-14	0.731	0
0.0	0	0.0	0	0	0.0	0	0	-15	0.743	0
-0.3	18.015	-0.3	0	0	-0.3	0	0	-16	0.754	0
-0.5	18.015	-0.5	0	0	-0.5	0	0	-17	0.763	0
-0.8	18.015	-0.8	0	0	-0.8	0	0	-18	0.771	0
-1.0	18.015	-1.0	0	0	-1.0	0	0	-19	0.000	0
-1.3	18.015	-1.3	0	0	-1.3	0	0	-20	0.916	0.084
-1.5	18.015	-1.5	0.007	0	-1.5	0	0	-21	0.916	0.084

-1.8	18.015	-1.8	0.124	0	-1.8	0	0	-22	0.916	0.084
-2.0	18.015	-2.0	0.210	0	-2.0	0	0	-23	0.916	0.084
-2.3	18.015	-2.3	0.276	0	-2.3	0	0	-24	0.916	0.084
-2.5	18.015	-2.5	0.328	0	-2.5	0	0	-25	0.916	0.084
-2.8	18.015	-2.8	0.370	0	-2.8	0	0			
-3.0	18.015	-3.0	0.405	0	-3.0	0	0			
-3.3	18.015	-3.3	0.435	0	-3.3	0	0			
-3.5	18.015	-3.5	0.460	0	-3.5	0	0			
-3.8	18.015	-3.8	0.482	0	-3.8	0	0			
-4.0	18.015	-4.0	0.501	0	-4.0	0.002	0			
-4.3	18.015	-4.3	0.000	0	-4.3	0.000				
-4.5	18.015	-4.5	0.765	0.235	-4.5	0.530	0.470			
-4.8	18.015	-4.8	0.765	0.235	-4.8	0.530	0.470			
-5.0	18.015	-5.0	0.765	0.235	-5.0	0.530	0.470			
-5.3	18.015	-5.3	0.765	0.235	-5.3	0.530	0.470			
-5.5	18.015	-5.5	0.765	0.235	-5.5	0.530	0.470			
-5.8	18.015	-5.8	0.765	0.235	-5.8	0.530	0.470			
-6.0	18.015	-6.0	0.765	0.235	-6.0	0.530	0.470			
-6.3	18.015	-6.3	0.765	0.235	-6.3	0.530	0.470			
-6.5	18.015	-6.5	0.765	0.235	-6.5	0.530	0.470			
-6.8	18.015	-6.8	0.765	0.235	-6.8	0.530	0.470			
-7.0	18.015	-7.0	0.765	0.235	-7.0	0.530	0.470			
-7.3	18.015	-7.3	0.765	0.235	-7.3	0.530	0.470			
-7.5	18.015	-7.5	0.765	0.235	-7.5	0.530	0.470			
-7.8	18.015	-7.8	0.765	0.235	-7.8	0.530	0.470			
-8.0	18.015	-8.0	0.765	0.235	-8.0	0.530	0.470			
-8.3	18.015	-8.3	0.765	0.235	-8.3	0.530	0.470			
-8.5	18.015	-8.5	0.765	0.235	-8.5	0.530	0.470			
-8.8	18.015	-8.8	0.765	0.235	-8.8	0.530	0.470			
-9.0	18.015	-9.0	0.765	0.235	-9.0	0.530	0.470			
-9.3	18.015	-9.3	0.765	0.235	-9.3	0.530	0.470			
-9.5	18.015	-9.5	0.765	0.235	-9.5	0.530	0.470			
-9.8	18.015	-9.8	0.765	0.235	-9.8	0.530	0.470			
-10.0	18.015	-10.0	0.765	0.235	-10.0	0.530	0.470			

Appendix E

Table E 1: Refractive index-water relationship (Using Equation 2-17)

Temp. (°C)	R. I	Temp. (°C)	R. I	Temp. (°C)	R. I	Temp. (°C)	R. I
-10	1.33403	1	1.33434	11	1.33402	21	1.33326
-9	1.33410	2	1.33433	12	1.33396	22	1.33316
-8	1.33416	3	1.33431	13	1.33390	23	1.33306
-7	1.33421	4	1.33429	14	1.33384	24	1.33295
-6	1.33425	5	1.33427	15	1.33377	25	1.33283
-5	1.33428	6	1.33424	16	1.33369	26	1.33271
-4	1.33431	7	1.33420	17	1.33362	27	1.33258
-3	1.33433	8	1.33416	18	1.33354	28	1.33244
-2	1.33434	9	1.33412	19	1.33345	29	1.33230
-1	1.33435	10	1.33407	20	1.33336	30	1.33215
0	1.33435						

Table E 2: Refractive Index-concentration relationship of Magnesium Sulphate at 20 °C **(Lide, 2010)**

Concentration (wt%)	Refractive index
0.5	1.334
1	1.335
2	1.3371
3	1.3391
4	1.3411
5	1.3431
6	1.3451
7	1.3471
8	1.3492
9	1.3512
10	1.3532
12	1.3572
14	1.3613
16	1.3654
18	1.3694
20	1.3735
22	1.3776
24	1.3817
26	1.3858

Table E 3: Refractive Index-temperature relationship of 8.4 wt% Magnesium Sulphate (Using Equation 2-18 and 19)

Temperature(°C)	Refractive Index
0	1.35176
2	1.35172
4	1.35167
6	1.35162
8	1.35157
10	1.35153
12	1.35148
14	1.35143
16	1.35138
18	1.35134
20	1.35129
22	1.35124
24	1.35119
26	1.35115
28	1.35110
30	1.35105

Appendix F

Matlab codes

F1: Filter generation (Payne & Mills, 2011)

```
close all
clear all

Nx = 100;
Ny = 100;

x = linspace(-1,1,Nx);
y = linspace(-1,1,Ny);
[X,Y] = meshgrid(x,y);

R = sqrt(X.^2 + Y.^2);
p=max(R);
n=max(p);
Rn=R./n; % normalises R so that values are between 0 and 1
colormap(hsv)
imagesc(Rn)
```

F2: Filter calibration

```
close
clear all

%Data
rad=2.35;%[mm]measured distance from centre
%filter image%
A=imread('D:\Old Data\Collected Data-Schlieren\Matlab
files\Filter image 5th March 3-0197','jpg');
Ahsv=rgb2hsv(A);
Ahue=Ahsv(:,:,1);

figure(1)
image(A)
figure(2)
imagesc(Ahue)% use to find centre point, (cx;cy)
```

```
cx=315; % from image(Ahue)
cy=252; % from image(Ahue)

%generate transmissivity function
vert=Ahue(:,cx); %vertical transmissivity
horiz=Ahue(cy,:); % horizontal transmissivity
s=size(Ahue); %dimensions of captured image [rows columns]

height=s(1);
width=s(2);

%graph%
%for vertical hue values
axisv=linspace(1,height,height);
figure(3)
plot(axisv,vert); ylabel('Hue'); xlabel('vertical position
through center (pixel)'); %use to get centre

axish= linspace(1,width,width);
huefuncv=vert(252:480);% find max and min from plot
shuev=length(huefuncv);
drv=linspace(0,rad,shuev); %% equating shue and shuev
figure(4)
plot(huefuncv,drv,'.'); xlabel('Hue'); ylabel('distance from
centre(mm) ');%title('vertical transmissivity');

shueh=length(huefuncv);
drh=linspace(rad,0,shueh);
angdrv=drv/400;

figure(5)
plot (huefuncv,angdrv);xlabel('Hue');ylabel('angle(radians)');
```

F3: Calculation of refractive index

```
clear all
close all

f2=400; % [mm]
L=5; % [mm]
rad=2.35; %radius of filter
pix=0.009351; % [mm] distance

%Schlieren image B
B1=imread ('C\1......jpeg');
B=B1 (270:450, :,:);
Bhsv=rgb2hsv (B);
Bh=Bhsv (: 1);

%Constants of calibration curve fit
  p1 = 1.511e+004;
  p2 = -3.461e+004;
  p3 = 3.137e+004;
  p4 = -1.432e+004;
  p5 =        3473;
  p6 =      -436.7;
  p7 =       27.95;
  p8 =     -0.3062;

%Calculation of distance
for i=1:180;
for j=1:640;
r=Bh (i, j);
dt (i, j) =p1*r^7 + p2*r^6 + p3*r^5 + p4*r^4 + p5*r^3 + p6*r^2
+ p7*r + p8;
end
end

theta=dt/f2;% finding the angle using distance and focal
length
dndr=theta/L;

figure (1);imagesc(B);
```

```
t=1:395;% defining distance from surface of heat exchanger or
surface of ice
y = mean(dndr(30:35,t),1); % getting the mean of dndr along t
y = y(y<0.0009); % Take off those values less than 0.0009
which were outliers due to scratches
t= t(y<0.0009); % Resizing t
V=dndr; %making a highlighted area  over which the measurement
is taken
V(30:35,t)=1.5e-4;% changing colour of the highlighted area
where dndr is mapped

B2=B(:,t,:);%cropping off ice and heater exchanger
Bh2=Bhsv(:,t,1);%cropping off ice and heater exchanger

y = y-min(y); %changing the negative gradient to positive

figure(2);imagesc(V);caxis ([0.5e-4 3.75e-
4]);colorbar;xlabel('Horizontal Pixel'),ylabel('Vertical
Pixel');

figure (3);plot(y);

figure(4)
y(390:end) = -y(390:end);
plot(y);xlabel('Pixel'); ylabel('Refractive Index Gradient');

dndrpf = polyfit(t,y(t),8);% fiiting a curve onto the dndr
intpf = polyint(dndrpf);%integrating the polyfit
int= polyval(intpf,t);
RI=int*0.01; % correcting the value according to boundary
conditions


figure(5);plot(t,int);xlabel('Pixel'); ylabel('Relative
Refractive Index ');

figure(6);plot(t,RI);xlabel('Pixel'); ylabel('Absolute
Refractive Index');
```

F4: Calculating of temperature of water

```
% relating refractive index to temperature using a quadratic
curve with max value of 1.3343

for j=1:395;
    N=RI(j);
a=-2e-006;
b=1e-008;
c=1.3343-N;
T_1=(-b+sqrt(b^2-4*a*c))/(2*a);
T_2=(-b-sqrt(b^2-4*a*c))/(2*a);
  if j<=390
     T(j)=T_2;
  else T(j)=T_1;
  end
end

pixels = (1:length(T));
pf=fliplr(pixels);
l = pix*(pixels-1);
l2=fliplr(l);%flipping the length

figure(7);plot(t,T); xlabel('Pixel'); ylabel('Temperature(
°C)');ylim([-10 22.5]);

figure(8);imagesc(B1);title('fullframe');

figure(9);imagesc(imrotate(B2,270));

figure(10);imagesc(V(:,t,:);
caxis ([0.5e-4 3.75e-]);colorbar;
xlabel('HorizontalPixel'),ylabel('Vertical Pixel');
```

Appendix G

Table G 1: Point Grey Research CCD Camera specifications

Specifications	
Autos	Off
Exposure	On
Brightness	0
Gamma	1.00
Shutter	62.017
Gain	2.778
Frame Rate	30fps
White Balance (Red)	89
White Balance (Blue)	81